Prognostics for Lithium-ion batteries for electric Vertical Take-off and Landing aircraft using data-driven machine learning

Mitici, Mihaela; Hennink, Birgitte ; Pavel, Marilena; Dong, Jianning

DOI
10.1016/j.egyai.2023.100233

Publication date
2023

Document Version
Final published version

Published in
Energy and AI

Energy and AI 12 (2023) 100233

Contents lists available at ScienceDirect

Energy and AI

journal homepage: www.elsevier.com/locate/egyai

Prognostics for Lithium-ion batteries for electric Vertical Take-off and Landing aircraft using data-driven machine learning

Mihaela Mitici [a,*], Birgitte Hennink [b], Marilena Pavel [b], Jianning Dong [c]

[a] Faculty of Science, Utrecht University, Heidelberglaan 8, 3584 CS, Utrecht, The Netherlands
[b] Faculty of Aerospace Engineering, Delft University of Technology, Kluyverweg 1, HS 2926, Delft, The Netherlands
[c] Electrical Engineering, Mathematics and Computer Science Faculty, TU Delft, 2628 CD, Delft, The Netherlands

HIGHLIGHTS

- Prognostics for batteries of electric Vertical Take-off and Landing aircraft.
- Estimating the Remaining-Useful-Life and State-of-Health of batteries.
- eVTOLs flying varying mission profiles.
- Feature importance quantification for RUL and SOH estimation.

GRAPHICAL ABSTRACT

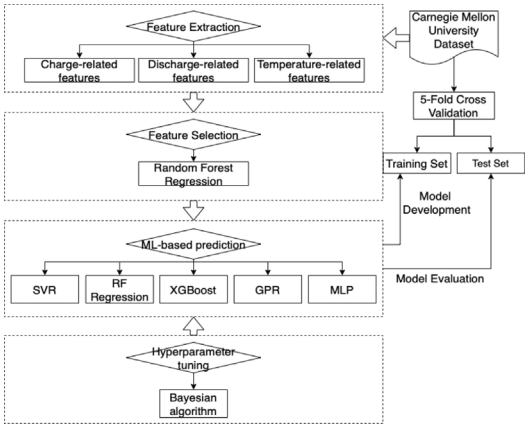

ARTICLE INFO

Keywords:
Electric Vertical Take-off and Landing vehicles
Lithium-ion battery
State-of-health
Machine learning
Remaining-useful-life

ABSTRACT

The health management of batteries is a key enabler for the adoption of Electric Vertical Take-off and Landing vehicles (eVTOLs). Currently, few studies consider the health management of eVTOL batteries. One distinct characteristic of batteries for eVTOLs is that the discharge rates are significantly larger during take-off and landing, compared with the battery discharge rates needed for automotives. Such discharge protocols are expected to impact the long-run health of batteries. This paper proposes a data-driven machine learning framework to estimate the state-of-health and remaining-useful-lifetime of eVTOL batteries under varying flight conditions and taking into account the entire flight profile of the eVTOLs. Three main features are considered for the assessment of the health of the batteries: charge, discharge and temperature. The importance of these features is also quantified. Considering battery charging before flight, a selection of missions for state-of-health and remaining-useful-lifetime prediction is performed. The results show that indeed, discharge-related features have the highest importance when predicting battery state-of-health and remaining-useful-lifetime. Using several machine learning algorithms, it is shown that the battery state-of-health and remaining-useful-life are well estimated using Random Forest regression and Extreme Gradient Boosting, respectively.

1. Introduction

Electric Vertical Take-off and Landing vehicles (eVTOLs) are seen as a solution to the growing traffic congestion in large cities, the traffic-related pollution and the inter-city connectivity needs. Several companies such as Airbus, Bell, Embraer, Joby Aviation, Kitty Hawk, Pipistrel, Volocopter, and Aurora Flight Sciences have been designing, building, and testing eVTOLs in the last few years [1].

* Corresponding author.
E-mail address: m.a.mitici@uu.nl (M. Mitici).

https://doi.org/10.1016/j.egyai.2023.100233
Received 11 November 2022; Received in revised form 17 January 2023; Accepted 20 January 2023
Available online 24 January 2023

The management of the batteries remains one of the challenges that the eVTOL industry faces today. The most frequently considered battery chemistry for e-mobility is lithium-ion due to its high energy-density, low self-discharge rates, and acceptable costs [2,3]. Several studies have focused on the health management of lithium-ion batteries for electric (on-ground) vehicles [4,5], on State-of-Health (SOH) estimation [6] and Remaining-Useful-Life (RUL) estimation [2,7]. The State-of-Charge (SOC) of the batteries has also been investigated in, for instance, [8,9]. The batteries considered in these studies have been subject to constant current (CC) and constant voltage (CV) charging with a constant discharge C-rates. For eVTOLs, however, the take-off and landing require larger discharge rates than the cruise phase. In the long-run, this is expected to have a direct impact on the health of the batteries. In turn, this is expected to influence the SOH and RUL of the batteries, which are sensitive to the long-run degradation trends of the batteries. Overall, given their safety-criticality and high cost, the batteries and their health management remains a priority for eVTOLs.

Several data-driven machine-learning approaches for battery RUL and SOH prediction have been proposed in the last years [10]. In [11] a hybrid method is proposed to estimate the RUL of fuel cells. The authors fuse particle filtering, to estimate the model parameters in the training phase, with a long-short term memory recurrent neural network to update the parameters in the prediction phase. In [12] a hybrid convolutional neural network with long short-term memory and a deep neural network are proposed to predict the lithium-ion battery RUL. The model has been validated using the dataset from NASA and Center for Advanced Life Cycle Engineering (CALCE). In [13] a unified deep learning method is proposed for RUL prediction. For this, a long short-term memory recurrent neural network has been developed to estimate the capacity of the battery. Within ten cycles, the RUL has been estimated with an error of only 0.13%.

For SOH estimation, many existing studies consider machine learning algorithms. In [14] a random forest is proposed to predict the SOH for Lithium-ion batteries of electric (on-ground) vehicles. The authors show that the average speed has a significant impact on the battery's health. In [15], a support vector machine is used for SOH estimation, leading to prediction errors of less than 2%. The authors argue that the SOH could be estimated using only the charge and discharge-related measurements. Also in this paper, we show that charge and discharge-related features have a high importance when estimating the SOH and RUL of batteries. Nevertheless, we show that the temperature at which the batteries are exposed to is also an important feature when predicting the SOH. A random forest regression is proposed in [16], achieving a Root Mean Square Error (RMSE) of 1.3%. The authors consider the charging voltage and the capacity measurements as features. In [17], a support vector machine is developed for SOH prediction, achieving an RMSE of 2.49%–3.62%. The authors show that the differential temperature curves during constant charging are of high importance for the SOH prediction.

Some of the most frequently used datasets for battery SOH and RUL predictions are [18–20], and [6,21]. For an extensive overview, please see [22]. These batteries, however, are subject to constant CC and CV cycling. For [20], lithium-ion batteries are charged and discharged at different temperatures, but still with a CC-CV charging protocol. The measured parameters are the capacity, internal resistance, voltage, current, and temperature [23]. For [18], LFP/Graphite cells are cycled. Here, the cells are always discharged at a 4 C-rate. For [6], the data was recorded during the actual usage of electric vehicles.

To the best of our knowledge, the dataset available at [24], which was released by Carnegie Mellon University, is the first battery dataset generated specifically for eVTOLs. In contrast with the previously discussed datasets, these batteries are subject to different C-rates during the discharge phase of a flight. Specifically, the take-off and landing of eVTOLs are performed at a larger C-rate than the cruise phase. Also, this eVTOL dataset cycles all battery cells until they reach EOL [24], instead of containing only early-cycle measurements, as is the case for [18]. All cells were tested in a Arbin 200 A cylindrical cell holder paired with a BioLogic BCS-815 modular battery cycler. Another novel aspect for this eVTOL dataset is that several parameters such as the temperature, power during discharge, and cruise length [24] are varied across multiple eVTOL missions.

Using the dataset provided in [24], a recent study [25] employed machine learning algorithms to predict the SOH of lithium-ion batteries for eVTOLs. Five machine learning algorithms have been assessed: Linear regression, linear support vector machines (SVM), k-nearest neighbors (kNN), random forest (RF) and light gradient boosting machine (LGBM). It was found that the kNN algorithm gives the best validation and test scores with the lowest training time. However, this study was performed using only the data recorded during the cruise phase of the flight. This is a strong limitation of the analysis, given that the vertical climb and descent are the most critical phases for the battery life of eVTOLs. The goal of the present study is to perform predictions for SOH and RUL of eVTOL batteries taking into account the entire mission profile of eVTOLs (i.e., both the take-off, climb, cruise, descent and landing). Moreover, we also identify which missions are actually relevant for SOH and RUL prediction. These are the missions where the battery is first charged to 100% SOC before performing a flight, which we refer to as a capacity test. This is relevant because the maximum available capacity test can determine the static capacity of the battery, which is critical when estimating the SOH of the battery. For practical applications, determining the real-time dynamic capacity is more important than determining the static capacity of the battery, since the real-time dynamic capacity can better reflect the battery's SOH. However, estimating the dynamic capacity accurately in real time is a challenge [26]. As a result, the regular static capacity calibration becomes an option and will be considered in this paper.

This paper proposed a framework to estimate the SOH and RUL of eVTOLs batteries using machine learning algorithms. We generate features based on measured variables and original voltage-capacity/time curves. These features are generated taking into account the charging and discharging protocols of the batteries, the temperature at which the batteries are exposed to, and the phase of the eVTOL mission (take-off/cruise/landing). Different from electric ground vehicles that require similar discharge rates throughout the entire trip, we show that for eVTOLs it is essential to perform feature engineering taking into account the phases of the missions. This is due to the fact that take-off and landing require large discharge rates than the cruise phase. We show that the variation in the voltage during take-off has the highest importance for both SOH and RUL prediction. This makes the take-off phase not only safety-critical from a flight perspective, but also of high importance for prognostics for batteries. Also different from the on-ground electric vehicles, we consider an End-of-Life (EOL) of 85%, instead of 80%, due to more rapid battery degradation observed for eVTOLs. We consider several machine learning algorithms for SOH and RUL prediction: Support Vector regression (SVR), Random Forrest (RF) regression, Gaussian Process regression (GPR), Extreme Gradient Boosting (XGBoost), and Multi-layer Perceptron (MLP). The results show that the RF regression has the best performance when predicting the SOH of the batteries, with an MAE of 1.33% and RMSE of 1.80%. For RUL prediction, the XGBoost leads to the best performance with an MAE of 54.53 missions and an RMSE of 67.92 missions. We also discuss the impact of the characteristics of the eVTOL mission on the battery SOH and RUL predictions. we show that the CC charging current is of high importance for RUL prediction, while the temperature and voltage are of high importance for SOH prediction.

The remainder of this paper is structured as follows. In Section 2, the dataset on eVTOL batteries is analyzed. The selection of the eVTOL missions to be considered for analysis is discussed in Section 3. In Section 4 a generic methodology for the prediction of the SOH and RUL of eVTOL batteries is introduced: the definition of SOH and RUL, feature engineering, the machine learning algorithms considered. In Section 5 this methodology is applied for SOH prediction. The results

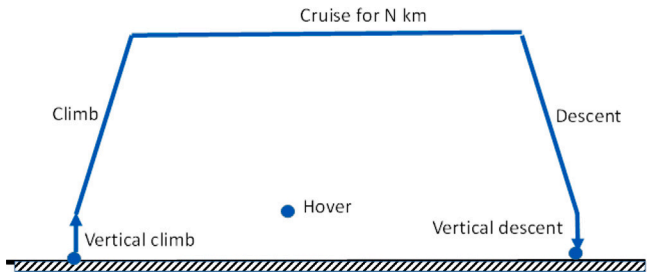

Fig. 1. Generic mission profile of an eVTOL.

obtained for SOH prediction are presented in Section 6 In Section 7 the methodology introduced in Section 4 is applied for RUL prediction. The results are presented in Section 8. In Section 9 the impact of the characteristics of the eVTOL missions on SOH and RUL prediction is discussed. Final conclusions are provided in Section 10.

2. Data description

We consider the health-monitoring dataset for Sony-Murata 18650 VTC-6 cell lithium-ion batteries available at [24]. These batteries are used to perform short-range missions with the Vahana eVTOL. Vahana is an eVTOL designed by Acubed (Airbus) for urban air mobility. It is an all-electric, single-seat, tilt-wing vehicle with a range of 50 km [27]. During cruise Vahana achieves an average speed of 190 km/h, with a maximum of 220 km/h. The longest flight performed by Vahana had a total duration of 19 min and 56 s [27].

Fig. 1 shows a generic mission profile for Vahana: vertical take-off, transition to forward flight, cruise for a specified distance, a transition back to a hover, and a vertical landing.

To discuss the dataset provided in [24], we define a mission profile for Vahana as a set of mission tasks whose specifications are unchanged across a sequence of missions. From the beginning to the end of a mission, these tasks are CC battery Charging phase, CV battery Charging phase, Rest period, eVTOL Take-off, eVTOL Cruise, eVTOL Landing, and a Rest period. Considering these tasks, dataset [24] contains 22 mission profiles (MP1–MP22), see Table 1.

Baseline mission profiles

Mission profiles VAH01, VAH17, and VAH27 are baseline mission profiles (see Table 1). We refer to them as baseline mission profiles because the other mission profiles are obtained by changing a mission task of one of these baseline mission profile.

Under a baseline mission profile, the battery is charged with 1 C-rate (CC charging phase). We note that a C-rate is a measure of the rate at which a battery is discharged relative to its maximum capacity. The CC charging phase ends as soon as the battery's voltage reaches 4.2 V. Then, the CV charging phase starts with a constant voltage of 4.2 V until the current is below $C/30$. After charging, the battery cell rests until the cell temperature reaches 35 °C. After this Rest period, the eVTOL performs a flight. The take-off has a duration of 75 s, with a discharge power of 54W, 5 C-rate, and 1.12Wh discharge energy. Afterwards, the cruise phase takes 800 s, at a discharge power of 16 W, 1.48 C-rate, and 3.55 Wh discharge energy. Then, the landing takes place with a duration of 105 s, a discharge power of 54 W, 5 C-rate, and 1.57 Wh discharge energy. Finally, the battery rests until its temperature decreases to 27 °C.

Table 1 shows the 22 mission profiles obtained by changing the following mission tasks of the baseline mission profiles: the duration of the cruise phase, the power used during flight (i.e., take-off, cruise, landing), the CC current, the CV voltage, and the ambient (chamber) temperature.

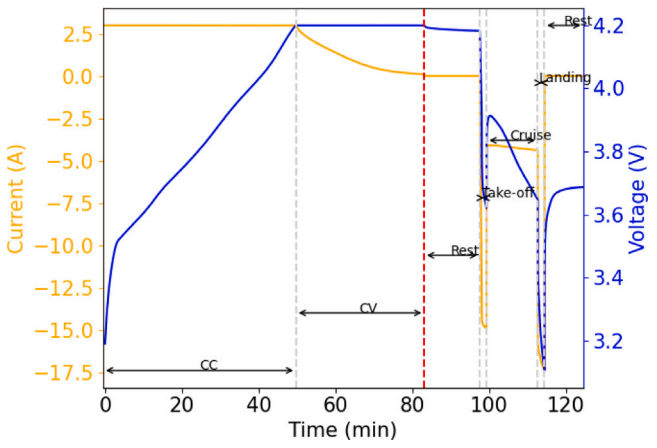

Fig. 2. Charging and discharging of 1st capacity test, VAH01. The battery is first discharged to 0% SOC, then is charged to 100% SOC. With 100% SOC, the 1st flight is performed. During take-off, cruise, landing, the battery is discharged.

Measurements

During every mission, the following measurements are recorded every time step: time (s), cell voltage (V), cell current (mA), energy supplied to the cell during charge (Wh), charge supplied to the cell during charge (mAh), energy extracted from the cell during discharge (Wh), charge extracted from the battery cell during discharge (mAh), cell surface temperature (°C), cycle number (-) and cycle segment (-).

Capacity tests

Given a mission profile, after every 50th mission, the residual battery charge is reduced to 0% SOC at a discharge rate of C/5 until the voltage drops below 2.5 V. Then, the battery is charged to 100% SOC at a charging rate of 1 C-rate and a constant voltage of 4.2 V. After the battery is fully charged, the eVTOL performs a flight (take-off, cruise, and landing). This "special" mission when the battery is charged to 100% and only afterwards the eVTOL takes off, is referred to as a capacity test. Table 1 shows the total number of capacity tests under each of the 22 mission profiles.

Fig. 2 shows the charging and discharging protocol of the first capacity test of VAH01. The CC charging phase in Fig. 2 has a duration of 50 min, and the battery is charged with 3.0 A. Afterwards, the CV charging phase takes place with 4.2 V for 33 min. The Rest period following charging has a duration of 14 min. The discharge phase starts with the take-off of the eVTOL. The duration of the take-off is 75 s. During take-off, the voltage drops from 3.92 V to 3.62 V. The cruise phase has a duration of 800 s. Hereafter, the landing phase has a duration of 105 s. During landing, the voltage drops from 3.57 V to 3.1 V. Finally, the mission ends with a Rest period of 605 s. At the end of the Rest period, the battery reaches a temperature of 27.3 °C.

To estimate the battery SOH and RUL, we consider the battery capacity during capacity tests only, i.e., when the battery is charged to 100% SOC before flight. We only focus on the capacity tests because dynamic capacity estimation would require an extensive analysis and hyperparameter tuning, which may be prone to estimation errors [26]. In contrast, a regular static capacity calibration is more reliable for testing purposes. The battery cell capacity during a cycle is given by the maximum amount of charge (in Ah) supplied to the cell during the charging phase of this cycle. In Fig. 2, the red dotted line shows the end of this charging phase of the 1st capacity test of VAH01.

Fig. 3 shows the mission immediately following the 1st capacity test of VAH01. It can be seen that the battery follows the same mission profile as in Fig. 2. However, the battery is now charged only from 3.8

Table 1
Mission profile characteristics, based on [24].

	Cruise duration	Power Take-off	Power Cruise	Power Landing	CC	CV	Ambient Temperature	VAH	#Missions	#Capacity tests
MP1	**800 s**	**54 W**	**16 W**	**54 W**	**1 C**	**4.2 V**	**25 °C**	**VAH01**	**847**	**17**
MP2	125% of 800 s	54 W	16 W	54 W	1 C	4.2 V	25 °C	VAH02	625	13
MP3	800 s	90% of 54 W	90% of 16 W	90% of 54 W	1 C	4.2 V	25 °C	VAH05	1615	31
MP4	800 s	54 W	16 W	54 W	50% of 1 C	4.2 V	25 °C	VAH06	9290	28
MP5	800 s	54 W	16 W	54 W	1 C	95.24% of 4.2 V	25 °C	VAH07	339	44
MP6	800 s	54 W	16 W	54 W	1 C	4.2 V	80% of 25 °C	VAH09	8527	46
MP7	800 s	54 W	16 W	54 W	1 C	4.2 V	120% of 25 °C	VAH10	1431	28
MP8	800 s	80% of 54 W	80% of 16 W	80% of 54 W	1 C	4.2 V	25 °C	VAH11	2249	44
MP9	50% of 800 s	54 W	16 W	54 W	1 C	4.2 V	25 °C	VAH12	2349	46
MP10	75% 800 s	54 W	16 W	54 W	1 C	4.2 V	25 °C	VAH13	1042	20
MP11	125% of 800 s	54 W	16 W	54 W	1 C	4.2 V	25 °C	VAH15	554	11
MP12	800 s	54 W	16 W	54 W	150% of 1 C	4.2 V	25 °C	VAH16	559	11
MP13	**800 s**	**54 W**	**16 W**	**54 W**	**1 C**	**4.2 V**	**25 °C**	**VAH17**	**1002**	**20**
MP14	800 s	54 W	16 W	54 W	150% of 1 C	4.2 V	25 °C	VAH20	611	12
MP15	125% of 800 s	54 W	16 W	54 W	1 C	4.2 V	25 °C	VAH22	579	12
MP16	800 s	54 W	16 W	54 W	1 C	97.62% of 4.2 V	25 °C	VAH23	697	13
MP17	800 s	54 W	16 W	54 W	50% of 1 C	4.2 V	25 °C	VAH24	801	16
MP18	800 s	54 W	16 W	54 W	1 C	4.2 V	80% of 25 °C	VAH25	554	11
MP19	75% of 800 s	54 W	16 W	54 W	1 C	4.2 V	25 °C	VAH26	1164	22
MP20	**800 s**	**54 W**	**16 W**	**54 W**	**1 C**	**4.2 V**	**25 °C**	**VAH27**	**587**	**12**
MP21	800 s	90% of 54 W	90% of 16 W	90% of 54 W	1 C	4.2 V	25 °C	VAH28	1182	23
MP22	800 s	54 W	16 W	54 W	1 C	4.2 V	140% of 25 °C	VAH30	919	18

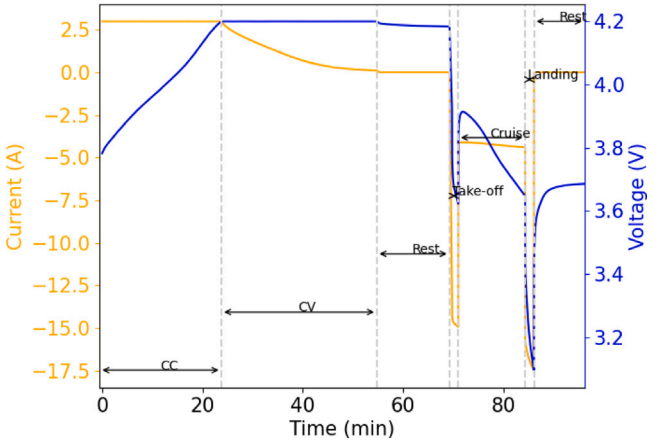

Fig. 3. Charging and discharging phase of the 2nd mission, mission profile VAH01.

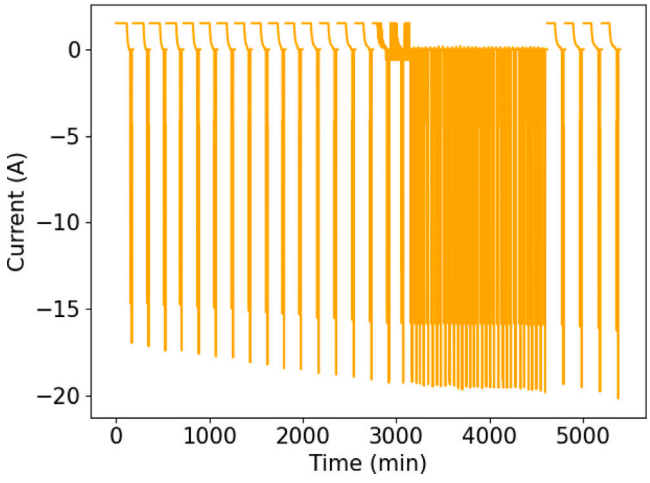

Fig. 4. Capacity tests — VAH06.

V to 4.2 V. As a result, the duration of the CC and CV charging period is shorter (83 min in the 1st capacity test vs. 55 min in this mission immediately following this 1st capacity test). In contrast, during the capacity test, the battery is charged from 3.2 V to 4.2V, and the CC and CV charging duration is more extensive (28 min).

3. Selection of mission profiles for the prediction of State-of-Health and Remaining-Useful-Life of eVTOL batteries

To estimate the SOH and RUL of eVTOL batteries, we consider only 19 mission profiles of the total 22 profiles (see Table 1). Mission profiles VAH06, VAH07, and VAH09 are not considered due to the inconsistencies in the battery characteristics recorded over time.

For VAH06, the degradation of the battery capacity follows an unexpected trend. During mission 766 (15th capacity test), the capacity of the battery is 2.51Ah. However, during the following capacity tests, from mission 903 until mission 8942, the battery's capacity varies between 1.8–1.9Ah. Afterwards, VAH06 consists of four standard capacity tests where the battery's capacity degrades from 2.51Ah to 2.44Ah (see also Fig. 4). This is unexpected as the battery's capacity should degrade over time, and not decrease and then increase again.

Fig. 5 shows the capacity tests for VAH07. Here, the battery's capacity increases over time as more capacity tests are performed. However, this pattern is unexpected since the battery's capacity is expected to decrease over time.

Fig. 6 shows the capacity tests for VAH09. For capacity tests corresponding to mission 728 until mission 6074, the battery capacity varies between 1.8–1.9Ah. Afterwards, from mission 6277 until mission 6306, the battery's capacity increases to 2.46Ah. Then, from mission 6480 until mission 8352, the capacity varies again between 1.8–1.9Ah. Finally, during the last two capacity tests, the battery's capacity degrades from

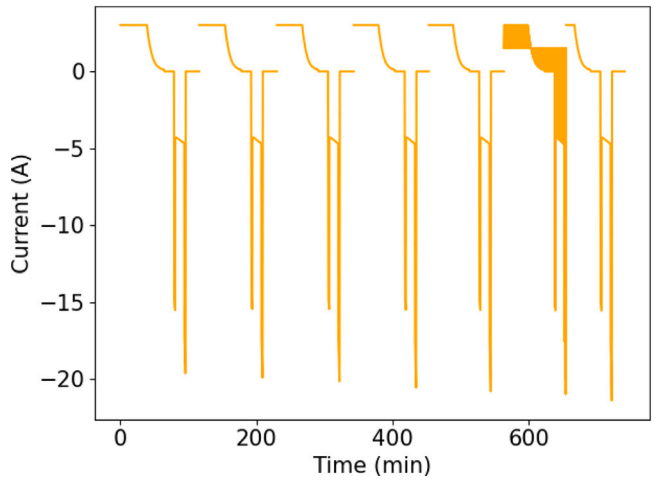

Fig. 5. Capacity tests — VAH07.

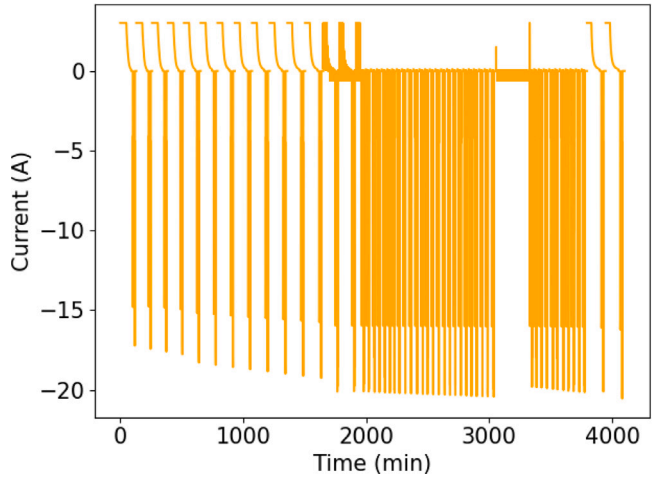

Fig. 6. Capacity tests — VAH09.

2.43 to 2.41Ah. This pattern is unexpected as we expect the capacity to decrease over time, and not to decrease, increase, and then decrease again.

In Appendix, the current during the capacity tests of the selected mission profiles is shown.

4. Methodology

In this section we propose a methodology to estimate the SOH and RUL of eVTOL batteries. First, we define the SOH and RUL of the batteries. Then, we perform feature engineering. Last, we propose a generic framework for SOH and RUL estimation of batteries using several machine learning algorithms.

4.1. Defining the State-of-Health and Remaining-Useful-Life for eVTOL batteries

In general, the SOH of a battery is defined as the ratio between the measured charging capacity during a capacity test, and the nominal capacity of the battery.

Although in [28] a nominal battery capacity of 3.0Ah is indicated in the dataset available at [24], all mission profiles, except VAH23, have a battery capacity of more than 3.0Ah during the first capacity test. For example, for mission profile VAH01, at the first capacity test, the battery has a capacity of 3.03Ah. For mission profile VAH23, the battery has a capacity of 2.71Ah during the first capacity test. Thus, a capacity of 3.0Ah does not seem to be the nominal capacity for all battery cells considered in [28]. Dataset [24] contains $Qcharge_i^{m,c}$ (mAh), the amount of charge supplied to the cell during charging. Therefore, we choose to determine the SOH of a battery as [29]:

$$SOH^{m,c} = \frac{\max_i(Qcharge_i^{m,c})}{\max_i(Qcharge_i^{m,0})} \cdot 100\%, \tag{1}$$

with $Qcharge_i^{m,c}$ the maximum measured capacity during a capacity test c of mission profile m, and $charge_i^{m,0}$ the maximum battery capacity measured during the first capacity test ($c = 0$) of mission profile m.

The remaining useful lifetime (RUL) of a battery is defined as the remaining number of missions/cycles for this battery until the End of Life (EOL), given that the battery has been used for $c >= 0$ missions. Formally, the RUL of a battery, estimated after c missions under mission profile m, is defined as:

$$RUL^{m,c} = T_{EOL}^{m} - T_{cc}^{m,c}, \tag{2}$$

with $T_{cc}^{m,c}$ the current mission/cycle number under mission profile m, and T_{EOL}^{m} the mission/cycle number when the battery capacity drops for the first time below an EOL-threshold under mission profile m.

Existing studies based on experimental battery measurements set the EOL-threshold to 80% of the nominal battery capacity [2,30–33]. To the best of our knowledge, EOL-thresholds for eVTOL batteries have not yet been formally established. For eVTOL batteries, it is expected that conservative safety margins will be considered. In [34], a conservative EOL-threshold of 85% of a nominal battery capacity of an eVTOL is considered. This eVTOL is designed for a total capacity of 5 persons with a range of 400 km [34]. Following [34], for our analysis, we also consider an EOL-threshold of 85% of the initially measured battery capacity.

The choice of the EOL-threshold has also an effect on the selection of the mission profiles. Using an EOL-threshold of 80%, not all mission profiles in the dataset [24] will have their batteries reaching EOL. Specifically, for mission profiles VAH01, VAH02, VAH15, VAH16, VAH20, VAH23, VAH24, VAH25, VAH27, and VAH28 the series of measurements stop before the battery capacity reaches 80% of the initially measured battery capacity. In other words, by using an EOL-threshold of 80% of the initial battery capacity, these mission profiles will not have run-to-EOL series of measurements.

Considering an EOL-threshold of 85% of the initially measured battery capacity, all mission profiles in dataset [24] have batteries that reach their EOL. Table 2 shows the number of missions until each

Table 2
Mission profiles and capacity tests, EOL-threshold 85% of initially measured battery capacity.

	Missions until EOL is reached	Capacity tests until EOL is reached
VAH01	613	13
VAH02	511	11
VAH05	766	16
VAH10	614	13
VAH11	817	17
VAH12	766	16
VAH13	562	12
VAH15	460	10
VAH16	460	10
VAH17	562	12
VAH20	460	10
VAH22	460	10
VAH23	562	12
VAH24	562	12
VAH25	513	11
VAH26	614	12
VAH27	512	11
VAH28	722	15
VAH30	511	11

battery reaches its EOL, and the number of capacity tests until these batteries reach their EOL.

4.2. Generating the features for SOH and RUL prediction based on [28]

To discuss the generation of features, let us first introduce some notations. Let C^m denote the number of capacity tests of a mission profile m, $1 \leq m \leq M$.

Let $t_s^{phase,m,c}$ and $t_e^{phase,m,c}$, $1 \leq m \leq M$, $1 \leq c \leq C^m$, denote the time step when phase $\in$ {take-off, cruise, landing} of capacity test c of mission profile m starts and ends, respectively.

Let $t_s^{charge,m,c}$ and $t_e^{charge,m,c}$, $1 \leq m \leq M$, $1 \leq c \leq C^m$, denote the time step when the charging phase of capacity test c of mission profile m starts and ends, respectively.

Let $T_i^{phase,m,c}$, $V_i^{phase,m,c}$, $Qdis_i^{phase,m,c}$ and $Qcharge_i^{m,c}$ denote the cell surface temperature, voltage, discharge and charge capacity, respectively, during a flight phase at time step i of capacity test c of mission profile m, with phase $\in$ {take-off, cruise, landing}, $t_s^{phase,m,c} \leq i \leq t_e^{phase,m,c}$, $1 \leq c \leq C^m$, $1 \leq m \leq M$.

We consider a total of 33 features (Table 3). These features are related to the charging, discharging and temperature of the battery, as follows.

Charge-related features

Fig. 7(a) shows the charging time vs. the charging voltage for the capacity tests of the baseline mission profile VAH01.

Mission profile VAH01 has 847 missions, out of which every 50th mission is a capacity test. Fig. 7(a) shows that as the number of missions increases, the duration of the CC charging phase decreases. The first capacity test has a CC charging duration of 50 min, whereas the last capacity test has a CC charging duration of 37 min. Hence, there is a 26% decrease in the CC charging duration. As the duration of the CC charging phase is reduced, the cut-off voltage of 4.2 V is reached earlier. Due to the lower duration of the CC charging phase, the CV charging phase begins earlier and has a longer duration. During the first capacity test, the CV charging phase takes 33 min. In contrast, the CV charging phase has a duration of 64 min during the last capacity test. Thus, for VAH01, the duration of the CV charging phase increases with 92%. The observed decrease in the CC charging duration and the increase of the CV charging duration over the number of missions is due to the battery polarization phenomenon [35]. Analyzing the charging of the battery, we consider as features: $\Delta^{CC,m,c}$, $\Delta^{CV,m,c}$, and $\Delta^{rest,m,c}$ (see Table 3).

Discharge-related features

Regarding discharge-related features, we consider features related to the discharge voltage of the battery, the discharge capacity, and the duration of each discharge phase (see Table 3).

Discharge voltage: Fig. 7(b) shows the discharge capacity vs. the discharge voltage during capacity tests of the baseline mission profile VAH01. For take-off and landing, a higher C-rate (5C) is considered than for cruise (1.48C). Fig. 7(b) shows that as the number of missions increases, the minimum discharge voltage decreases during each flight phase. Also, during take-off and landing, the discharge voltage drop is higher than during cruise. This is expected since the take-off and landing are performed at a higher C-rate.

Since the discharge voltage varies for every flight phase and across capacity tests, we aim to capture the impact of these variations by considering voltage-related features. Thus, we consider the following battery-discharge related features: $V_{max}^{phase,m,c}$, $V_{min}^{phase,m,c}$, $V_{mean}^{phase,m,c}$, and $V_{var}^{phase,m,c}$ (see Table 3).

These voltage-related featured are considered since they reflect the open circuit voltage and internal resistance, which are closely related to the remaining capacity and the aging of the battery [26,36].

Discharge capacity: Fig. 7(b) shows that the discharge capacity increases from take-off to cruise to landing. The discharge capacity also increases as the number of missions increases. To capture these patterns, we consider the following features related to the discharge capacity of the battery (see also Table 3): $Qdis_{max}^{phase,m,c}$, $Qdis_{min}^{phase,m,c}$, $Qdis_{mean}^{phase,m,c}$, and $Qdis_{var}^{phase,m,c}$ (see Table 3).

The discharge capacity and its variation reflect the load characteristics of the battery, which directly impacts the aging of the battery. As such, we consider as features the maximum, minimum, mean and variance of the discharge capacity.

Duration of the discharge phase: We consider $\Delta^{phase,m,c}$, the duration of each discharge phase $\in$ {take-off, landing, cruise} of capacity test c of mission profile m (see also Table 3). Since the cruise duration varies across mission profiles, we also consider the duration of the cruise phase as a feature.

Temperature-related features

Fig. 7(c) shows the maximum, minimum, and average cell surface battery temperature recorded during all missions of mission profile VAH01, with a total of 17 capacity tests. We note that for missions 1–343, the temperature is recorded at an average interval of 4.7 s. For missions 344 and onwards, the temperature is measured at an average interval of 22.9 s. During every capacity test, the maximum and average temperature decrease abruptly. This is because the battery cell is allowed to rest at the end of a capacity test until the temperature reduces to 27 °C. Fig. 7(c) also shows that, as the battery is used for a longer time, its maximum temperature increases.

During a capacity test, Fig. 7(d) shows that the highest cell surface temperature is reached during landing. Fig. 7(d) also shows that the temperature reaches a peak during take-off and decreases during cruise. In Fig. 7(d), the tasks of the first capacity test are highlighted in orange, while the last capacity test is highlighted in blue. When considering both the take-off, landing, and cruise phases, the temperature increases as the number of capacity tests increases.

To capture the change in battery surface temperature as more missions are performed, we consider as feature $T_{max}^{phase,m,c}$ which is recorded during the discharge phase $\in$ {take-off, landing, cruise} of capacity test c of each mission profile m, see also Table 3.

4.3. Generic framework for SOH and RUL prediction of eVTOL batteries using machine learning

Fig. 8 shows the framework considered for estimating the SOH and RUL of eVTOL batteries. We first generate features (see Section 4.2) based on charge-related, discharge-related, and temperature-related battery measurements. We next select those features with the highest importance for SOH and RUL prediction. With the selected features, we estimate SOH and RUL using the following machine learning algorithms: support vector regression (SVR), random forest (RF) regression, Extreme Gradient Boosting (XGBoost), Gaussian Process Regression (GPR), and Multi-layer Perceptron (MLP). The hyperparameters of these algorithms are also tuned using a Bayesian hyperparameter tuning algorithm. The SOH and RUL of the batteries are obtained using a 5-fold cross validation. Below is a short description of the five machine learning algorithms considered.

SVR is a supervised machine learning algorithm based on kernels [37]. SVR is considered a suitable algorithm for SOH/RUL estimation because it excels at characterizing nonlinear relationships between inputs and outputs [15]. This is also the case for your analysis, where we expect a non-linear degradation of the battery capacity.

The RF regression is a supervised ensemble machine learning model that combines heterogeneous decision trees [38]. Only a randomly selected portion of the training set is used to construct each forest tree. RF regression uses averaging to improve the prediction accuracy and control over-fitting [39].

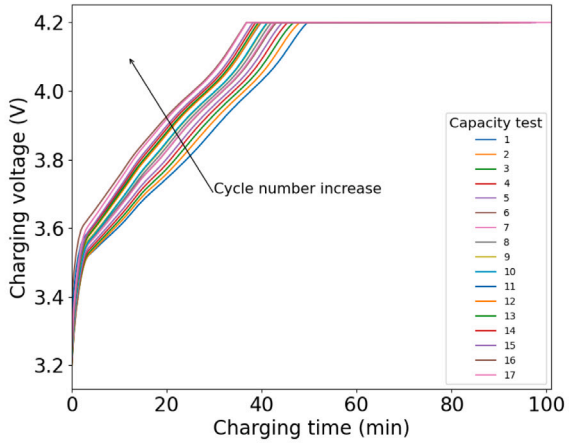

(a) Charging curves during all capacity tests - VAH01.

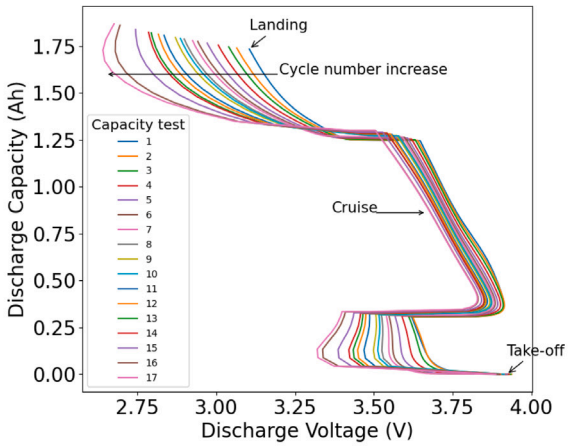

(b) Discharge capacity during all capacity tests - VAH01.

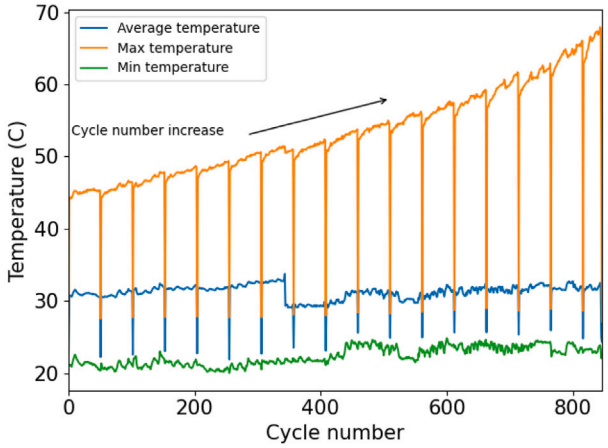

(c) Average, max, min battery cell surface temperature during all missions - VAH01.

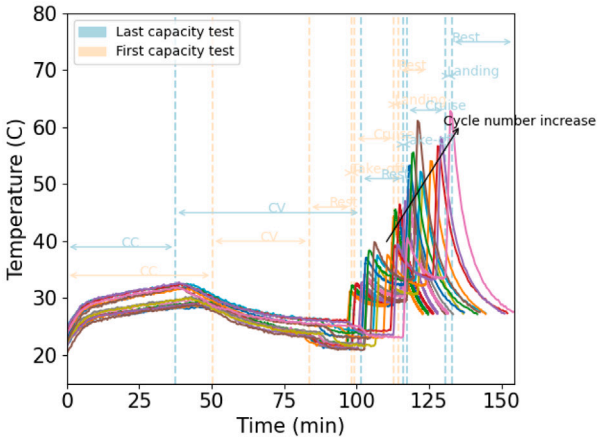

(d) Battery cell surface temperature during all capacity tests - VAH01.

Fig. 7. Capacity tests — VAH01.

Table 3
Charge-related, discharge-related and temperature-related features.

Feature	Unit	Description	Formula
$\Delta^{CC,m,c}$	[s]	Duration CC charging phase of capacity test c of mission m	
$\Delta^{CV,m,c}$	[s]	Duration CV charging phase of capacity test c of mission m	
$\Delta^{rest,m,c}$	[s]	Duration rest phase after charging of capacity test c of mission m	
$\Delta^{phase,m,c}$	[s]	Duration flight phase of capacity test c of mission m	
$V_{max}^{phase,m,c}$	[V]	Maximum voltage during flight phase of capacity test c of mission m	
$V_{min}^{phase,m,c}$	[V]	Minimum voltage during flight phase of capacity test c of mission m	
$V_{mean}^{phase,m,c}$	[V]	Mean voltage during flight phase of capacity test c of mission m	$\frac{1}{t_e - t_s + 1} \sum_{t_s}^{t_e} V_i^{phase,m,c}$, $1 \leq m \leq M, 1 \leq c \leq C^m$
$V_{var}^{phase,m,c}$	[V]	Variance voltage during flight phase of capacity test c of mission m	
$Qdis_{max}^{phase,m,c}$	[Ah]	Maximum discharge capacity during flight phase of capacity test c of mission m	
$Qdis_{min}^{phase,m,c}$	[Ah]	Minimum discharge capacity during flight phase of capacity test c of mission m	
$Qdis_{mean}^{phase,m,c}$	[Ah]	Mean discharge capacity during flight phase of capacity test c of mission m	$\frac{1}{t_e - t_s + 1} \sum_{t_s}^{t_e} Qdis_i^{phase,m,c}$, $1 \leq m \leq M, 1 \leq c \leq C^m$
$Qdis_{var}^{phase,m,c}$	[Ah]	Variance discharge capacity during flight phase of capacity test c of mission m	
$T_{max}^{phase,m,c}$	[°C]	Maximum battery cell surface temperature during flight phase of capacity test c of mission m	

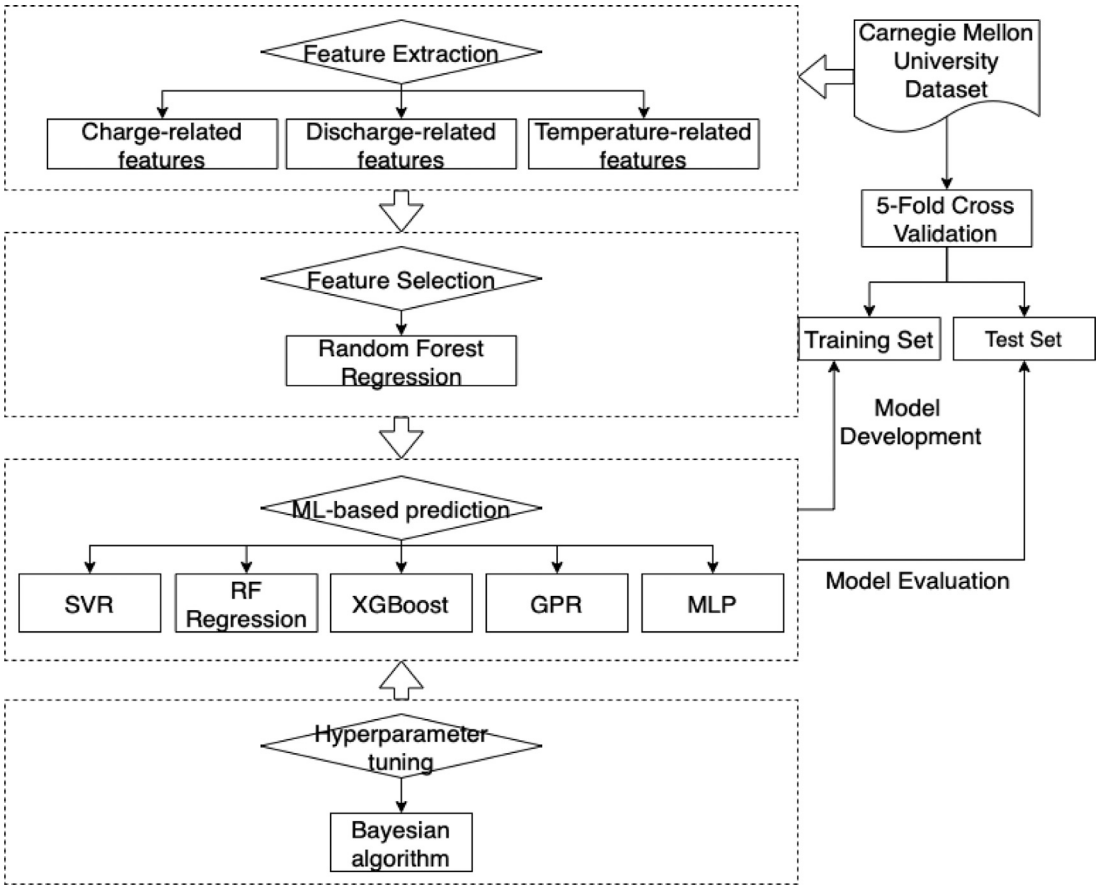

Fig. 8. Generic framework for predicting the SOH and RUL of batteries using machine learning algorithms.

XGBoost is a gradient-boosted decision-tree-based ensemble machine learning algorithm. XGBoost is based on an optimized distributed gradient boosting, i.e., it makes use of parallel tree boosting to improve performance and speed [40]. Unlike decision trees, each regression tree of XCBoost contains a continuous score on each leaf, and additional regularization terms help to smooth the final learned weights to avoid over-fitting, i.e, it makes use of a built-in regularization [9,40].

GPR is a probabilistic non-parametric kernel-based model [41,42]. GPR is based on a kernel that predicts the output by incorporating prior knowledge and obtaining a hypothesis of posterior probability via a Bayesian approach. GPR has the advantages of adaptive hyper-parameter acquisition and it has been shown to obtain a similar performance when compared with neural networks and SVM [43].

MLP is a feed-forward neural network with multiple layers and adaptive weights [44,45]. All hidden layers include batch normalization to improve the neural network's stability.

5. Predicting the State-of-Health of eVTOL batteries

In this section we apply the methodology introduced in Section 4 to estimate the SOH of eVTOL batteries.

5.1. Feature selection and feature importance quantification

In Section 4.2, a total of 33 features have been considered. From these 33 features, we select for SOH prediction only the features with high importance. The importance of the features is obtained using a random forest regression model.

Based on the importance of the 33 features considered, we select the top 65% (i.e., 21) features with the highest importance (see Fig. 9). The variance of the voltage during take-off has the highest importance, followed by the minimum voltage during take-off, and the duration of the CC charging phase. The results show that the features related to take-off have a high importance. This can be explained by the fact that the battery experiences a high discharge voltage during take-off. During high discharge voltages, the internal resistance increases, which impacts the SOH [46]. Also, the duration of the CC charging phase has a high importance for the prediction of the SOH. As the battery performs more missions, the SOH decreases while the duration of the CC charging phase increases (see Fig. 7(a)).

Fig. 9 shows that the variance of the voltage during take-off has the highest importance, followed by the minimum voltage during take-off, and the duration of the CC charging phase. The results show that the features related to take-off have a high importance, This can be explained by the fact that the battery experiences a high discharge voltage during take-off. During high discharge voltages, the internal resistance increases, which impacts the SOH [46]. Also, the duration of the CC charging phase has a high importance for the prediction of the SOH. As the battery performs more missions, the SOH decreases while the duration of the CC charging phase increases (see Fig. 7(a)).

5.2. Setup for the machine learning algorithms

5-fold cross-validation

Using the framework in Section 4.3, we employ a 5-fold cross validation to estimate the SOH of the batteries. The folds are generated using group K-fold such that each fold contains a unique set of mission profiles used for testing. In each fold, the number of mission profiles selected for testing is approximately the same (3–4 mission profiles per fold). Also, the number of capacity tests of these selected 3–4 mission profiles is approximately the same (75 capacity tests used for testing). Having a total of 19 mission profiles (see Section 2) with a total of

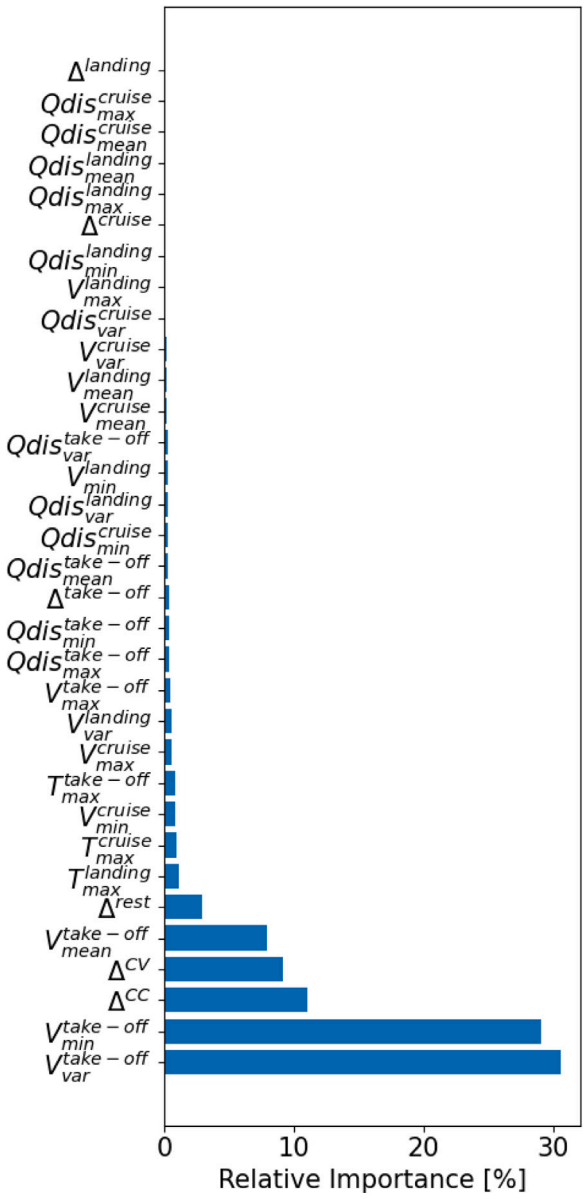

Fig. 9. Feature importance — SOH estimation.

380 capacity tests, we aim to allocate mission profiles to folds such that each of the 5 folds contains approximately 380/5 capacity tests available for testing. Each mission profile is allocated to one and only one fold. Indeed, the number of capacity tests available for testing in each fold varies between 74–84 capacity tests per fold. We obtain the following 5 folds used for testing:

- Fold 1: the test dataset consists of mission profiles VAH12, VAH22, VAH24.
- Fold 2: the test dataset consists of mission profiles VAH11, VAH27, VAH30.
- Fold 3: the test dataset consists of mission profiles VAH02, VAH05, VAH13, VAH15.
- Fold 4: the test dataset consists of mission profiles VAH10, VAH17, VAH20, VAH23.
- Fold 5: the test dataset consists of mission profiles VAH01, VAH16, VAH26, VAH28.

Table 4
Optimized hyperparameters — SOH.

	Hyperparameters
SVR	$Kernel = Linear$ $Tolerance = 0.186$
RF Regression	$Trees = 797$ $MaxDepth = 30$ $MinSampleLeaf = 2$ $MinSampleSplit = 4$
XGBoost	$Trees = 3100$ $MaxDepth = 19$ $LearningRate = 0.25$ $Subsample = 0.80$
GPR	$Alpha = 0.069$ $Kernel = Dotproduct + Whitekernel$
MLP	$BatchSize = 96$ $Neurons1st\ Layer = 90$ $Neurons2nd\ Layer = 90$ $Neurons3rd\ Layer = 40$

Hyperparameter tuning

Table 4 shows the optimal hyperparameters obtained for each of the five machine learning algorithms considered. We performed hyperparameter tuning based on a Bayesian optimization algorithm [2].

5.3. Performance metrics

For every mission profile used for testing, we predict the SOH at each capacity test. The performance of our SOH predictions is evaluated using the Mean Absolute Error (MAE), Root Mean Squared Error (RMSE), and the Mean Absolute Percentage Error (MAPE). These metrics are defined, for the estimated SOH of a battery under mission profile $m, 1 \leq m \leq M$, as follows:

$$MAE^{m}_{SOH} = \frac{1}{C^m}\sum_{i=1}^{C^m} |SOH^{m,i} - \hat{SOH}^{m,i}|,$$

$$RMSE^{m}_{SOH} = \sqrt{\frac{1}{C^m}\sum_{i=1}^{C^m}\left(\hat{SOH}^{m,i} - SOH^{m,i}\right)^2}$$

$$MAPE^{m}_{SOH} = \frac{1}{C^m}\sum_{i=1}^{C^m}\frac{|SOH^{m,i} - \hat{SOH}^{m,i}|}{SOH^{m,i}} \cdot 100\%,$$

where $SOH^{m,i}$ is the true battery SOH at capacity test i of mission profile m, $\hat{SOH}^{m,i}$ is the predicted SOH at capacity test i of mission profile $m, 1 \leq m \leq M$.

The overall performance of our SOH predictions across all M mission profiles is evaluated using:

$$MAE_{SOH} = \frac{1}{M}\sum_{j=1}^{M} MAE^{j}_{SOH}$$

$$RMSE_{SOH} = \frac{1}{M}\sum_{j=1}^{M} RMSE^{j}_{SOH}$$

$$MAPE_{SOH} = \frac{1}{M}\sum_{j=1}^{M} MAPE^{j}_{SOH}$$

6. Results — State-of-Health prediction for eVTOL batteries

Table 5 shows the MAE, RMSE, and MAPE obtained across all mission profiles for SOH estimation.

Table 6 shows the MAE, RMSE, and MAPE obtained for SOH prediction for each mission profile. The last row of Table 6 gives the average of these metrics. The results show that the SOH estimation errors obtained for the baseline mission profiles are below the average MAE,

Table 5
Results — predicting SOH [%].

	MAE	RMSE	MAPE
SVR	1.48	2.20	0.02
RF Regression	**1.33**	**1.80**	**0.02**
XGBoost	1.39	1.91	0.02
GPR	1.48	2.27	0.79
MLP	2.75	7.49	0.03

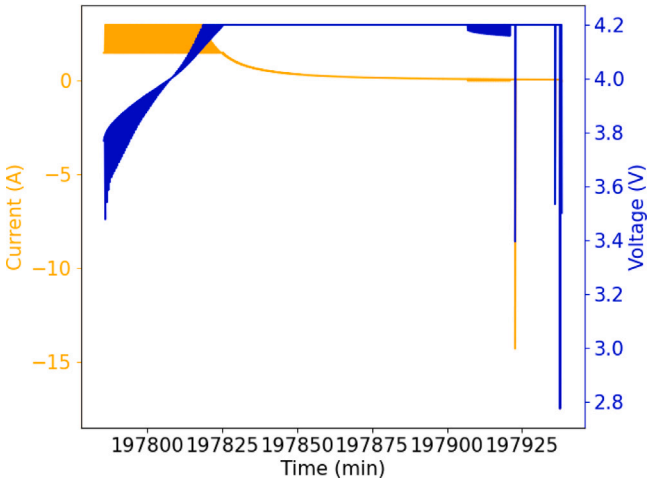

Fig. 10. Second to last capacity test — VAH05.

RMSE and MAPE. The lowest prediction errors are obtained for mission profiles VAH02, VAH10, VAH12, VAH13, VAH15, VAH16, VAH26 and VAH28, when considering the RF regression.

The highest prediction errors are obtained for VAH05, regardless of the machine algorithms considered (see Table 6). For the second to last capacity test of VAH05, the RF regression predicts a SOH of 88.98%, whereas the true SOH is 76.29%. For the last capacity test of VAH05, the RF regression predicts the SOH to be 72.63%, while the true SOH is 56.21%. The high SOH prediction errors for VAH05 for the second to last capacity test can be explained by analyzing the current and voltage during that specific second to last capacity test (see Fig. 15(c)). Fig. 10 shows the second last to capacity test of VAH05. Fig. 10 shows that the current oscillates during the CC phase. Also, the current during the discharge phases does not follow the pattern of standard capacity tests (see Fig. 2). In fact, during discharge, the voltage exhibits 4 peaks. The second-highest value of the RMSE, when using RF regression, is achieved for mission profile VAH22 (see Table 6). Fig. 15(l) shows that during the second to last capacity test of VAH22, the current does not follow the pattern of a standard capacity test. During the second to last capacity test of VAH22, the SOH is estimated to be 89.79%, while the true SOH is 82.64%. The SOH for the last capacity test is estimated to be 80.21%, while the true SOH is 69.53%. This could be explained by the fact that the current and voltage oscillate during the charging, take-off, cruise and landing of the second capacity test of VAH22 (see Fig. 11).

Table 7 shows the intermediate errors obtained for SOH prediction when employing RF regression, which is the best performing machine learning algorithm among all five considered (see Table 5). The number of capacity tests differs across the eVTOLs since each battery reaches its EOL at a different moment in time. This is a result of the type of missions each eVTOL performs. Overall, the results show that the SOH is consistently well estimated as the number of missions performed increases.

7. Predicting the remaining useful life of eVTOL batteries

In this section we apply the methodology introduced in Section 4 to estimate the RUL of eVTOL batteries.

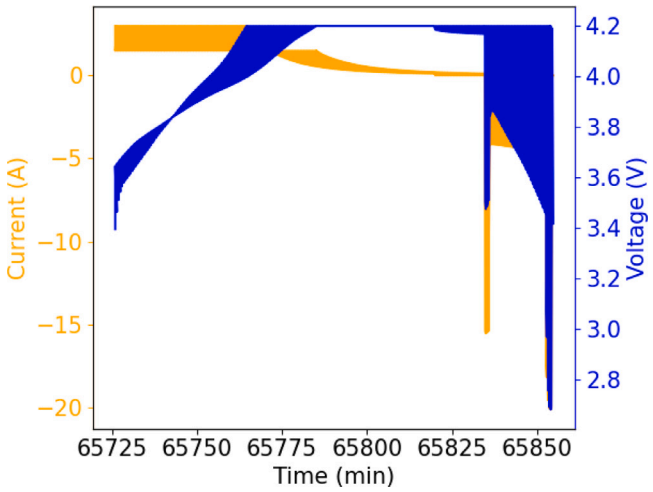

Fig. 11. Second to last capacity test — VAH22.

7.1. Feature selection and feature importance quantification

In Section 4.2, 33 features have been generated. In this section we quantify the importance of the features for RUL prediction using a RF regression model. We select the top 65% (21 features) with the highest importance (see Fig. 12). The results shows that the mean and the variance of the voltage during take-off are the most important features. This is expected since the take-off is performed at a high C-rate, which leads to a high internal impedance during take-off. In turn, a higher internal impedance is expected to affect the remaining life of the battery. The voltage during landing, cruise, as well as the duration of the CC charging phase are also shown to be of high importance for RUL estimation.

7.2. Setup for the machine learning algorithms

5-fold cross-validation

Using the framework in Section 4.3, we employ a 5-fold cross validation to estimate the battery RUL. Compared with the estimation of SOH, where a total of 380 capacity tests are considered, for RUL estimation, only 215 capacity tests are considered. This is because we consider an EOL of 85% of the initially measured battery capacity.

The 5 folds are generated using group K-fold such that each fold contains a unique set of mission profiles used for testing. In each fold, the number of mission profiles selected for testing is approximately the same (4 mission profiles per fold). Also, the number of capacity tests of these selected 4 mission profiles is approximately the same (45 capacity tests used for testing). Thus, having a total of 19 mission profiles (see Section 2) with a total of 215 capacity tests, we aim to allocate mission profiles to folds such that each of the 5 folds contains approximately 215/5 capacity tests used for testing. Each mission profile is allocated to one and only one fold. We obtain the following 5 folds for testing:

- Fold 1: the test dataset consists of mission profiles VAH11, VAH16, VAH20, VAH24.
- Fold 2: the test dataset consists of mission profiles VAH05, VAH15, VAH17, VAH26.
- Fold 3: the test dataset consists of mission profiles VAH02, VAH12, VAH23, VAH27.
- Fold 4: the test dataset consists of mission profiles VAH10, VAH28, VAH30.
- Fold 5: the test dataset consists of mission profiles VAH01, VAH13, VAH22, VAH25.

Table 6
Error metrics SOH [%].

	SVR			**RF Regression**			XGBoost			GPR			MLP		
	MAE	RMSE	MAPE	MAE	RMSE	MAPE	MAE	RMSE	MAPE	MAE	RMSE	MAPE	MAE	RMSE	MAPE
VAH01	1.09	1.47	0.01	1.29	1.51	0.01	1.2	1.53	0.01	1.18	1.57	0.01	2.14	2.3	0.02
VAH02	0.89	1.07	0.01	0.85	1.01	0.01	2.13	2.64	0.02	0.61	0.85	0.01	1.91	2.2	0.02
VAH05	2.82	7.62	0.04	1.82	3.88	0.03	2.02	3.85	0.03	3.04	9.74	0.04	18.36	94.69	0.24
VAH10	0.55	0.71	0.01	0.87	1.01	0.01	0.86	1.04	0.01	0.65	0.87	0.01	2.08	2.44	0.03
VAH11	1.79	1.91	0.02	1.51	1.7	0.02	1.92	2.41	0.02	1.33	1.49	0.02	1.47	1.69	0.02
VAH12	2.78	2.99	0.04	0.65	0.84	0.01	0.91	1.16	0.01	3.52	3.73	0.04	1.71	1.9	0.02
VAH13	0.87	1.13	0.01	0.58	0.71	0.01	0.84	1.07	0.01	0.89	1.09	0.01	1.12	1.55	0.01
VAH15	1.0	1.2	0.01	0.31	0.46	0.0	0.72	1.03	0.01	0.79	0.98	0.01	1.75	2.03	0.02
VAH16	0.66	1.13	0.01	1.26	1.45	0.01	0.82	0.97	0.01	0.65	1.05	0.01	0.7	1.03	0.01
VAH17	1.24	1.4	0.01	0.46	0.63	0.01	1.08	1.4	0.01	0.89	1.07	0.01	0.56	0.86	0.01
VAH20	1.13	1.44	0.01	1.85	2.34	0.02	1.17	1.53	0.01	0.92	1.25	0.01	0.78	1.19	0.01
VAH22	2.54	5.52	0.03	1.79	3.74	0.02	1.95	4.19	0.03	2.02	4.72	0.02	5.21	12.92	0.07
VAH23	2.11	2.72	0.02	2.95	3.74	0.03	2.45	3.19	0.03	2.31	2.69	0.03	7.27	7.62	0.08
VAH24	3.9	4.0	0.04	1.55	2.08	0.02	2.55	2.71	0.03	4.28	4.39	0.05	1.19	1.48	0.01
VAH25	0.94	1.62	0.01	2.0	2.71	0.02	1.85	2.46	0.02	0.86	1.44	0.01	2.06	2.76	0.02
VAH26	1.32	2.14	0.02	1.17	1.64	0.01	0.8	1.31	0.01	1.5	2.35	0.02	1.34	2.11	0.02
VAH27	1.33	1.84	0.01	1.03	1.32	0.01	1.05	1.39	0.01	1.46	1.9	0.02	1.21	1.64	0.01
VAH28	0.63	1.07	0.01	0.89	1.1	0.01	0.69	0.86	0.01	0.61	1.14	0.01	0.57	0.86	0.01
VAH30	0.56	0.8	0.01	2.36	2.43	0.03	1.36	1.58	0.02	0.63	0.82	0.01	0.89	1.04	0.01
Average	1.48	2.20	0.02	1.33	1.80	0.02	1.39	1.91	0.02	1.48	2.27	0.02	2.75	7.49	0.03

Table 7
Results — predicting SOH [%] at each capacity test using RF Regression, N.A.= Non-Applicable.

		Capacity Test									
		1st [%]	5th [%]	10th [%]	15th [%]	20th [%]	25th [%]	30th [%]	35th [%]	40th [%]	45th [%]
VAH01	Predicted SOH	96.90%	91.31%	85.93%	80.89%	N.A.	N.A.	N.A.	N.A.	N.A.	N.A.
	True SOH	100.00%	91.85%	86.83%	82.66%	N.A.	N.A.	N.A.	N.A.	N.A.	N.A.
VAH02	Predicted SOH	98.36%	91.88%	85.15%	N.A.	N.A.	N.A.	N.A.	N.A.	N.A.	N.A.
	True SOH	100%	91.14%	85.52%	N.A.	N.A.	N.A.	N.A.	N.A.	N.A.	N.A.
VAH05	Predicted SOH	98.42%	94.37%	88.52%	84.31%	82.25%	77.85%	88.98%	N.A.	N.A.	N.A.
	True SOH	100%	92.84%	88.22%	85.14%	82.53%	79.33%	76.29%	N.A.	N.A.	N.A.
VAH10	Predicted SOH	97.82%	92.99%	87.24%	83.71%	80.68%	77.32%	N.A.	N.A.	N.A.	N.A.
	True SOH	100%	91.87%	86.72%	83.16%	79.63%	76.49%	N.A.	N.A.	N.A.	N.A.
VAH11	Predicted SOH	98.69%	93.94%	91.62%	88.09%	84.74%	81.42%	78.86%	76.32%	71.81%	
	True SOH	100%	93.25%	89.26%	86.48%	82.20%	80.05%	77.70%	75.62%	73.01%	N.A.
VAH12	Predicted SOH	99.19%	92.01%	88.26%	84.96%	80.78%	79.33%	77.96%	75.19%	73.54%	70.68%
	True SOH	100%	92.89%	88.53%	85.34%	81.28%	78.31%	75.89%	75.03%	73.69%	71.61%
VAH13	Predicted SOH	99.12%	92.96%	88.04%	82.87%	N.A.	N.A.	N.A.	N.A.	N.A.	N.A.
	True SOH	100%	92.52%	87.64%	84.20%	N.A.	N.A.	N.A.	N.A.	N.A.	N.A.
VAH15	Predicted SOH	98.72%	90.69%	84.93%	N.A.	N.A.	N.A.	N.A.	N.A.	N.A.	N.A.
	True SOH	100%	90.87%	84.76%	N.A.	N.A.	N.A.	N.A.	N.A.	N.A.	N.A.
VAH16	Predicted SOH	96.81%	91.97%	83.91%	N.A.	N.A.	N.A.	N.A.	N.A.	N.A.	N.A.
	True SOH	100%	91.24%	84.92%	N.A.	N.A.	N.A.	N.A.	N.A.	N.A.	N.A.
VAH17	Predicted SOH	98.84%	91.75%	86.78%	83.10%	N.A.	N.A.	N.A.	N.A.	N.A.	N.A.
	True SOH	100%	91.74%	86.31%	82.34%	N.A.	N.A.	N.A.	N.A.	N.A.	N.A.
VAH20	Predicted SOH	95.91%	89.48%	81.49%	N.A.	N.A.	N.A.	N.A.	N.A.	N.A.	N.A.
	True SOH	100%	90.89%	84.08%	N.A.	N.A.	N.A.	N.A.	N.A.	N.A.	N.A.
VAH22	Predicted SOH	98.96%	90.38%	84.48%	N.A.	N.A.	N.A.	N.A.	N.A.	N.A.	N.A.
	True SOH	100%	90.82%	84.59%	N.A.	N.A.	N.A.	N.A.	N.A.	N.A.	N.A.
VAH23	Predicted SOH	90.84%	89.19%	88.49%	N.A.	N.A.	N.A.	N.A.	N.A.	N.A.	N.A.
	True SOH	100%	91.25%	85.95%	N.A.	N.A.	N.A.	N.A.	N.A.	N.A.	N.A.
VAH24	Predicted SOH	98.82%	95.81%	87.32%	81.45%	N.A.	N.A.	N.A.	N.A.	N.A.	N.A.
	True SOH	100%	91.95%	86.72%	82.18%	N.A.	N.A.	N.A.	N.A.	N.A.	N.A.
VAH25	Predicted SOH	96.18%	90.17%	94.01%	N.A.	N.A.	N.A.	N.A.	N.A.	N.A.	N.A.
	True SOH	100%	91.94%	86.85%	N.A.	N.A.	N.A.	N.A.	N.A.	N.A.	N.A.
VAH26	Predicted SOH	97.41%	92.42%	87.52%	81.47%	77.27%	N.A.	N.A.	N.A.	N.A.	
	True SOH	100%	92.34%	87.38%	82.55%	78.82%	N.A.	N.A.	N.A.	N.A.	N.A.
VAH27	Predicted SOH	99.12%	91.82%	84.73%	N.A.	N.A.	N.A.	N.A.	N.A.	N.A.	N.A.
	True SOH	100%	91.10%	85.51%	N.A.	N.A.	N.A.	N.A.	N.A.	N.A.	N.A.
VAH28	Predicted SOH	96.80%	91.82%	87.76%	83.71%	81.44%	N.A.	N.A.	N.A.	N.A.	N.A.
	True SOH	100%	92.68%	87.92%	84.36%	81.78%	N.A.	N.A.	N.A.	N.A.	N.A.
VAH30	Predicted SOH	98.20%	93.99%	87.79%	83.87%	N.A.	N.A.	N.A.	N.A.	N.A.	N.A.
	True SOH	100%	91.40%	85.77%	81.52%	N.A.	N.A.	N.A.	N.A.	N.A.	N.A.

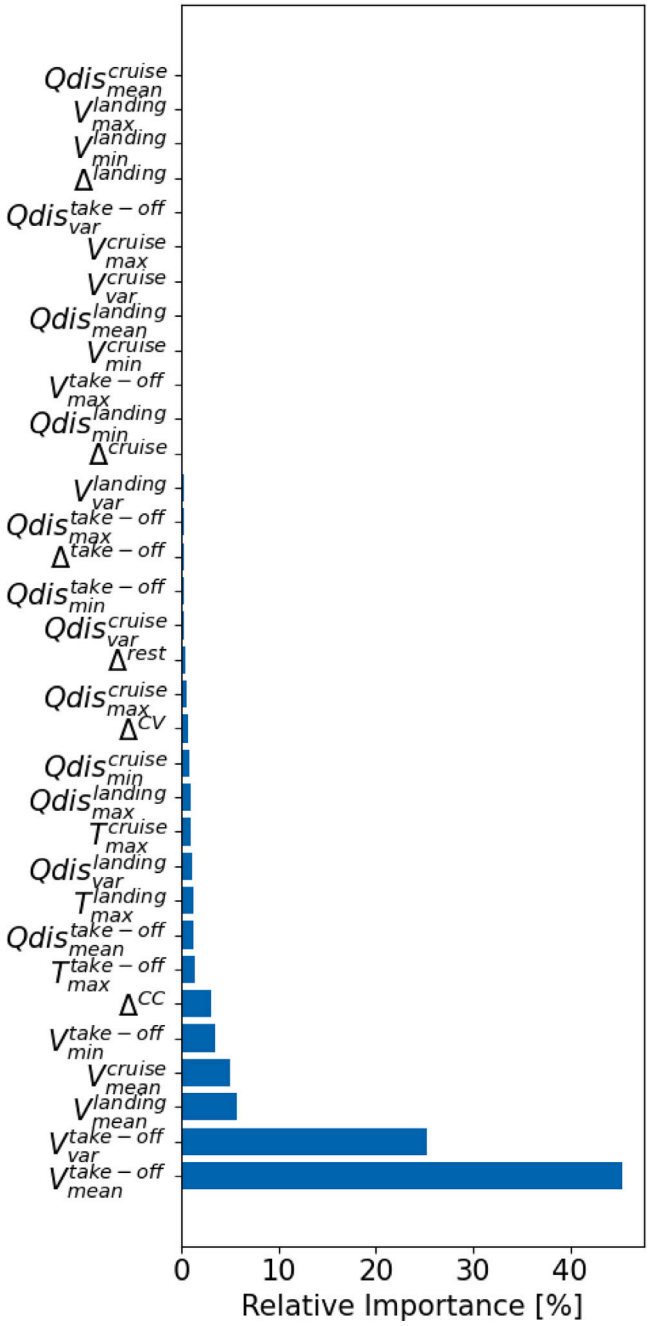

Fig. 12. Feature importance — RUL estimation.

Hyperparameter tuning

Table 8 shows the optimal hyperparameters obtained for each machine learning algorithm considered. The hyperparameter tuning is based on the Hyperopt Bayesian algorithm [47].

7.3. Performance metrics

For every mission profile used for testing, we predict the RUL at each capacity test. The performance of the RUL predictions is evaluated using the Mean Absolute Error (MAE), Root Mean Squared Error (RMSE), and the Mean Absolute Percentage Error (MAPE). These performance metrics are defined for the estimated RUL of a battery under mission profile $m, 1 \leq m \leq M$, as follows:

$$MAE_{RUL}^{m} = \frac{1}{C^m} \sum_{i=1}^{C^m} |RUL^{m,i} - \hat{RUL}^{m,i}|,$$

$$RMSE_{RUL}^{m} = \sqrt{\frac{1}{C^m} \sum_{i=1}^{C^m} \left(\hat{RUL}^{m,i} - RUL^{m,i}\right)^2}$$

$$MAPE_{RUL}^{m} = \frac{1}{C^m} \sum_{i=1}^{C^m} \frac{|RUL^{m,i} - \hat{RUL}^{m,i}|}{RUL^{m,i}} \cdot 100\%,$$

where $RUL^{m,i}$ is the true battery RUL at capacity test i of mission profile m, $\hat{RUL}^{m,i}$ is the predicted RUL at capacity test c of mission profile $m, 1 \leq m \leq M$.

The overall performance of our RUL predictions across all M mission profiles is evaluated using:

$$MAE_{RUL} = \frac{1}{M} \sum_{j=1}^{M} MAE_{RUL}^{j}$$

$$RMSE_{RUL} = \frac{1}{M} \sum_{j=1}^{M} RMSE_{RUL}^{j}$$

$$MAPE_{RUL} = \frac{1}{M} \sum_{j=1}^{M} MAPE_{RUL}^{j}$$

Table 8
Optimized hyperparameters — RUL.

	Hyperparameters
SVR	$Kernel = linear$ $Tolerance = 88.75$
RF Regression	$Trees = 1951$ $MaxDepth = 104$ $MinSampleLeaf = 3$ $MinSampleSplit = 2$
XGBoost	$Trees = 5100$ $MaxDepth = 29$ $LearningRate = 0.25$ $Subsample = 0.91$
GPR	$Alpha = 1.0$ $Kernel = RationalQuadratic$
MLP	$BatchSize = 64$ $Neurons 1^{st} Layer = 40$ $Neurons 2^{nd} Layer = 10$ $Neurons 3^{rd} Layer = 30$

Table 9
Results — RUL prediction [#missions].

	MAE	RMSE	MAPE
SVR	66.48	79.03	0.38
RF Regression	63.25	75.81	0.39
XGBoost	**54.53**	**67.92**	**0.39**
GPR	59.37	72.86	0.27
MLP	75.45	87.97	0.44

8. Results — remaining useful life prediction for eVTOL batteries

Table 9 shows the MAE, RMSE, and MAPE obtained when considering all 19 mission profiles. From all considered machine learning algorithms, XGBoost leads to the lowest RUL estimation errors.

Table 10 shows the MAE, RMSE, and MAPE obtained for RUL estimation. In the last row, the average MAE, RMSE, and MAPE for each algorithm is given.

The results show that the lowest RUL estimation errors (MAE, RMSE) are obtained using XGBoost, and for mission profiles with an increase in the cruise duration (VAH02, VAH15, VAH22) or a 50% increase of the CC charging current (VAH16 and VAH20).

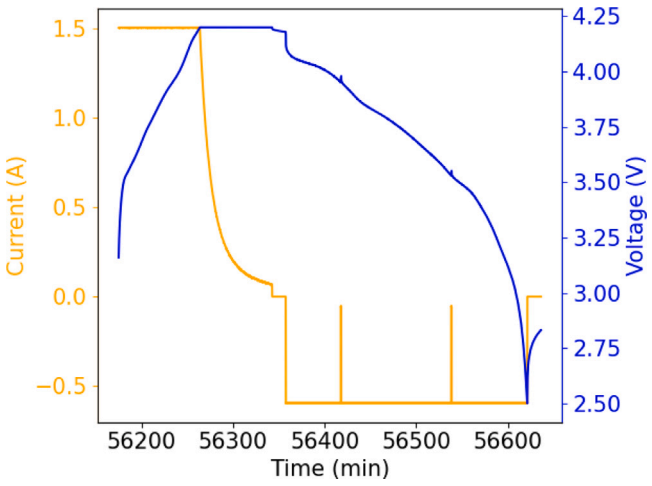

Fig. 13. Second to last capacity test — VAH25.

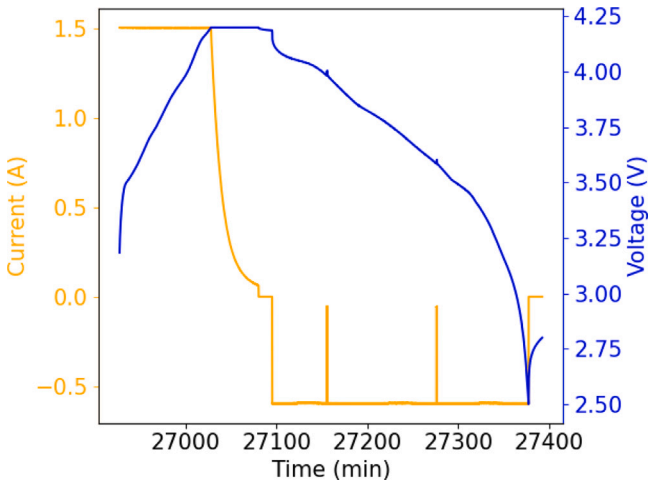

Fig. 14. Second to last capacity test — VAH28.

Table 10 also shows that the highest RUL prediction errors are obtained for VAH11. Mission profile VAH11 has the largest power reduction (20%) during take-off, cruise, and landing.

Compared with the results obtained for SOH prediction, RUL prediction errors are significantly lower for mission profiles VAH05 and VAH22. This is because the EOL (85% of the initially measured capacity) of the batteries used for VAH05 and VAH22 is reached before the non-standard capacity tests of VAH05 and VAH22.

For mission profile VAH25, XGBoost leads to RUL estimation errors above average. This can be explained by the non-standard second to last capacity test in VAH25. In Fig. 13, the second to last capacity test of VAH25 is plotted with respect to the voltage considered. Fig. 13 shows that the capacity test follows a different pattern than the standard capacity tests (see Fig. 2). The CC charging current is lower, and the discharge phases are not clearly distinguishable. The reason behind it is that sduring the second to last capacity test, two capacity tests have been performed one after the other. Yet, these have been reported as only one capacity test in the dataset provided in [24]. For this second to last capacity test, the RUL is estimated to be 434 missions, while the true RUL is 52 missions. This large error for this capacity test increases significantly the overall RUL prediction error for this mission profile.

XGBoost also leads to large RUL estimation errors for mission profile VAH28. VAH28 has a 10% power reduction during take-off, cruise, and landing, compared with the baseline mission profiles. These results can be explained by the fact that the 6th capacity test of this mission profile exhibits abnormal trends. Also here, two capacity tests have been performed one after the other, but these have been reported as only one capacity test in dataset [24]. Fig. 14 shows the current and voltage during the 6th capacity test. Fig. 14 shows that the CC charging current is lower compared to the standard capacity tests (see Fig. 2). Besides, the current and voltage during the discharge phases do not follow the pattern of the standard capacity tests (see Fig. 2). During the discharge phase, the take-off, cruise, and landing cannot be clearly distinguished. For this 6th capacity test, the RUL is estimated to be 148 missions, while the true RUL is 466 missions. Also here, these large errors obtained for an early capacity test increase the overall RUL estimation errors for this mission.

Table 11 shows the RUL prediction errors obtained at every capacity test. Also here, the number of capacity tests differs for every eVTOL since the EOL of the battery is reached at the different moment in time for each battery. The results show that the prediction errors are smaller in the initial phase of the eVTOL usage. In general, after the 7th capacity tests, all prediction errors increase for all eVTOLs.

9. The impact of mission characteristics on the estimation of the State-Of-Health and Remaining Useful Life of eVTOL batteries

One of the mission characteristics that is varied across mission profiles is the duration of the cruise phase. Mission profiles VAH02, VAH15, and VAH22 have a cruise phase extended by 25% compared to the baseline mission profiles. Mission profiles VAH12, VAH13, and VAH26 have a 50%, 25% and 25% shorter cruise duration, respectively, compared with the baseline mission profiles.

When estimating SOH using RF regression, the estimation errors (MAE, RMSE, MAPE) for these mission profiles are below the average estimation errors (see Table 6). The exception is mission profile VAH22, where the second to last capacity test exhibits unexpected patterns in the voltage and the current of the charging and discharging phases (see also Fig. 11). In this case study, thus, after increasing or decreasing the duration of the cruise phase, the SOH is still well estimated.

The importance of the duration of the cruise phase for SOH estimation was ranked as low in Section 5.1. This does not mean that the characteristics of the cruise phase are of no importance for SOH estimation. In fact, the following features related to the cruise phase have been ranked as having a high importance (in decreasing order of importance): maximum temperature during cruise, minimum voltage during cruise, maximum voltage during cruise, and minimum discharge capacity during cruise. The results show that the maximum temperature during cruise is of high importance for SOH estimation. This is also in accordance with existing literature [48,49] where the battery temperature is shown to be highly correlated with the SOH of the battery.

Similarly, when considering the RUL estimation using XGBoost, the RUL estimation errors for mission profiles VAH02, VAH15, VAH22 are below the average errors. Also in this case, the feature regarding cruise duration, Δ^{cruise}, is shown to have a low importance for RUL estimation (see Section 7.1). Nonetheless, several features related to cruise phase have been shown to have a high importance for RUL prediction. In decreasing order of importance, the following features have been selected for RUL estimation: mean voltage during cruise, maximum discharge capacity during cruise, variance discharge capacity during cruise, minimum discharge capacity during cruise, and maximum temperature during cruise.

Another mission characteristic that has been varied across several mission profiles is the CC charging current. Mission profiles VAH16 and VAH20 have a 50% increase of the CC charging current, while VAH24 has a 50% reduction of the CC charging current when compared to the baseline mission profiles. For both VAH16, VAH20 and VAH24,

Table 10
Error metrics RUL prediction [#missions], EOL-threshold 85% of battery capacity.

	SVR			RF Regression			**XGBoost**			GPR			MLP		
	MAE	RMSE	MAPE	MAE	RMSE	MAPE	MAE	RMSE	MAPE	MAE	RMSE	MAPE	MAE	RMSE	MAPE
VAH01	99.21	104.42	0.53	105.72	117.74	0.34	62.64	75.85	0.28	70.28	80.3	0.32	69.91	85.41	0.42
VAH02	37.21	48.7	0.32	53.49	67.41	0.24	52.72	57.54	0.22	23.26	30.66	0.1	80.52	87.69	0.33
VAH05	75.78	91.53	0.32	34.48	45.09	0.15	35.99	47.14	0.12	24.38	34.42	0.14	121.01	129.48	0.63
VAH10	29.19	34.14	0.2	30.16	34.62	0.22	36.43	43.5	0.15	82.54	96.59	0.27	47.57	52.29	0.2
VAH11	139.37	173.13	0.96	163.78	187.94	0.98	199.58	224.73	1.1	145.87	173.34	0.71	367.18	383.3	1.93
VAH12	114.59	138.36	0.29	102.78	114.45	0.31	97.43	109.16	0.28	133.43	155.36	0.32	38.82	44.07	0.14
VAH13	52.43	61.41	0.19	20.87	25.01	0.1	24.91	28.7	0.11	16.94	18.96	0.07	27.3	32.41	0.14
VAH15	12.17	15.9	0.1	22.02	25.92	0.18	18.15	23.79	0.14	14.13	18.55	0.12	13.87	19.83	0.14
VAH16	67.75	70.88	0.41	50.78	55.66	0.32	30.77	34.77	0.21	73.73	75.08	0.43	74.94	89.47	0.34
VAH17	40.64	49.44	0.25	36.31	40.37	0.18	26.18	31.57	0.19	22.81	31.52	0.21	43.31	48.81	0.31
VAH20	59.21	61.67	0.41	41.84	46.07	0.31	19.63	27.21	0.18	63.19	63.93	0.39	66.32	78.78	0.25
VAH22	10.37	12.5	0.06	28.92	32.25	0.17	8.76	14.41	0.07	12.54	15.86	0.11	7.12	9.28	0.07
VAH23	133.27	169.15	0.38	126.67	149.08	0.94	115.34	131.3	0.67	124.96	154.4	0.41	129.93	145.97	0.85
VAH24	40.19	43.46	0.23	62.81	79.2	0.54	45.09	56.82	0.37	72.57	94.38	0.29	87.77	106.45	0.74
VAH25	69.66	112.77	0.82	73.85	161.69	1.09	65.27	126.31	0.88	29.14	44.76	0.33	72.94	114.6	0.74
VAH26	58.81	70.97	0.4	28.62	31.21	0.18	31.7	35.01	0.17	36.94	41.49	0.23	60.3	65.11	0.27
VAH27	55.31	59.54	0.38	13.3	17.67	0.09	14.91	19.19	0.06	36.07	41.73	0.14	30.45	34.06	0.13
VAH28	66.99	80.77	0.34	53.92	57.31	0.2	49.74	91.25	0.17	75.56	128.24	0.25	68.73	111.97	0.47
VAH30	100.98	102.77	0.66	151.42	151.74	0.9	100.76	112.24	0.75	69.77	84.71	0.32	25.63	32.51	0.19
Average	66.48	79.03	0.38	63.25	75.81	0.39	54.53	67.92	0.32	59.37	72.86	0.27	75.45	87.97	0.44

Table 11
Results RUL prediction [#missions] at each capacity test using XGBoost, N.A.= Non-Applicable.

		Capacity Test							
		1st [#missions]	3rd [#missions]	5th [#missions]	7th [#missions]	9th [#missions]	11th [#missions]	13th [#missions]	15th [#missions]
VAH01	Predicted RUL	484	458	401	279	67	46	N.A.	N.A.
	True RUL	612	510	408	306	204	102	N.A.	N.A.
VAH02	Predicted RUL	568	451	375	273	78	N.A.	N.A.	N.A.
	True RUL	510	408	306	204	102	N.A.	N.A.	N.A.
VAH05	Predicted RUL	656	617	573	460	417	314	198	N.A.
	True RUL	765	663	561	459	357	255	153	N.A.
VAH10	Predicted RUL	597	449	392	279	246	110	N.A.	N.A.
	True RUL	613	511	409	306	204	102	N.A.	N.A.
VAH11	Predicted RUL	757	764	737	695	621	575	520	369
	True RUL	816	714	612	510	408	306	204	102
VAH12	Predicted RUL	643	532	382	305	200	228	87	N.A.
	True RUL	765	663	561	459	357	255	153	N.A.
VAH13	Predicted RUL	681	596	405	324	262	122	N.A.	N.A.
	True RUL	663	561	459	357	255	153	N.A.	N.A.
VAH15	Predicted RUL	460	365	238	141	N.A.	N.A.	N.A.	N.A.
	True RUL	459	357	255	153	N.A.	N.A.	N.A.	N.A.
VAH16	Predicted RUL	479	415	277	208	N.A.	N.A.	N.A.	N.A.
	True RUL	459	357	255	153	N.A.	N.A.	N.A.	N.A.
VAH17	Predicted RUL	516	443	345	255	177	N.A.	N.A.	N.A.
	True RUL	561	459	357	255	153	N.A.	N.A.	N.A.
VAH20	Predicted RUL	450	349	250	199	N.A.	N.A.	N.A.	N.A.
	True RUL	459	357	255	153	N.A.	N.A.	N.A.	N.A.
VAH22	Predicted RUL	460	356	249	147	N.A.	N.A.	N.A.	N.A.
	True RUL	459	357	255	153	N.A.	N.A.	N.A.	N.A.
VAH23	Predicted RUL	303	343	290	210	252	N.A.	N.A.	N.A.
	True RUL	561	459	357	255	153	N.A.	N.A.	N.A.
VAH24	Predicted RUL	499	417	324	266	219	N.A.	N.A.	N.A.
	True RUL	561	459	357	255	153	N.A.	N.A.	N.A.
VAH25	Predicted RUL	454	413	299	161	36	N.A.	N.A.	N.A.
	True RUL	512	410	307	205	103	N.A.	N.A.	N.A.
VAH26	Predicted RUL	665	554	446	265	178	N.A.	N.A.	N.A.
	True RUL	613	511	409	255	153	N.A.	N.A.	N.A.
VAH27	Predicted RUL	548	408	330	135	N.A.	N.A.	N.A.	N.A.
	True RUL	511	409	307	153	N.A.	N.A.	N.A.	N.A.
VAH28	Predicted RUL	691	603	512	347	297	166	100	N.A.
	True RUL	721	619	517	414	312	210	108	N.A.
VAH30	Predicted RUL	654	423	384	317	262	N.A.	N.A.	N.A.
	True RUL	510	408	306	204	102	N.A.	N.A.	N.A.

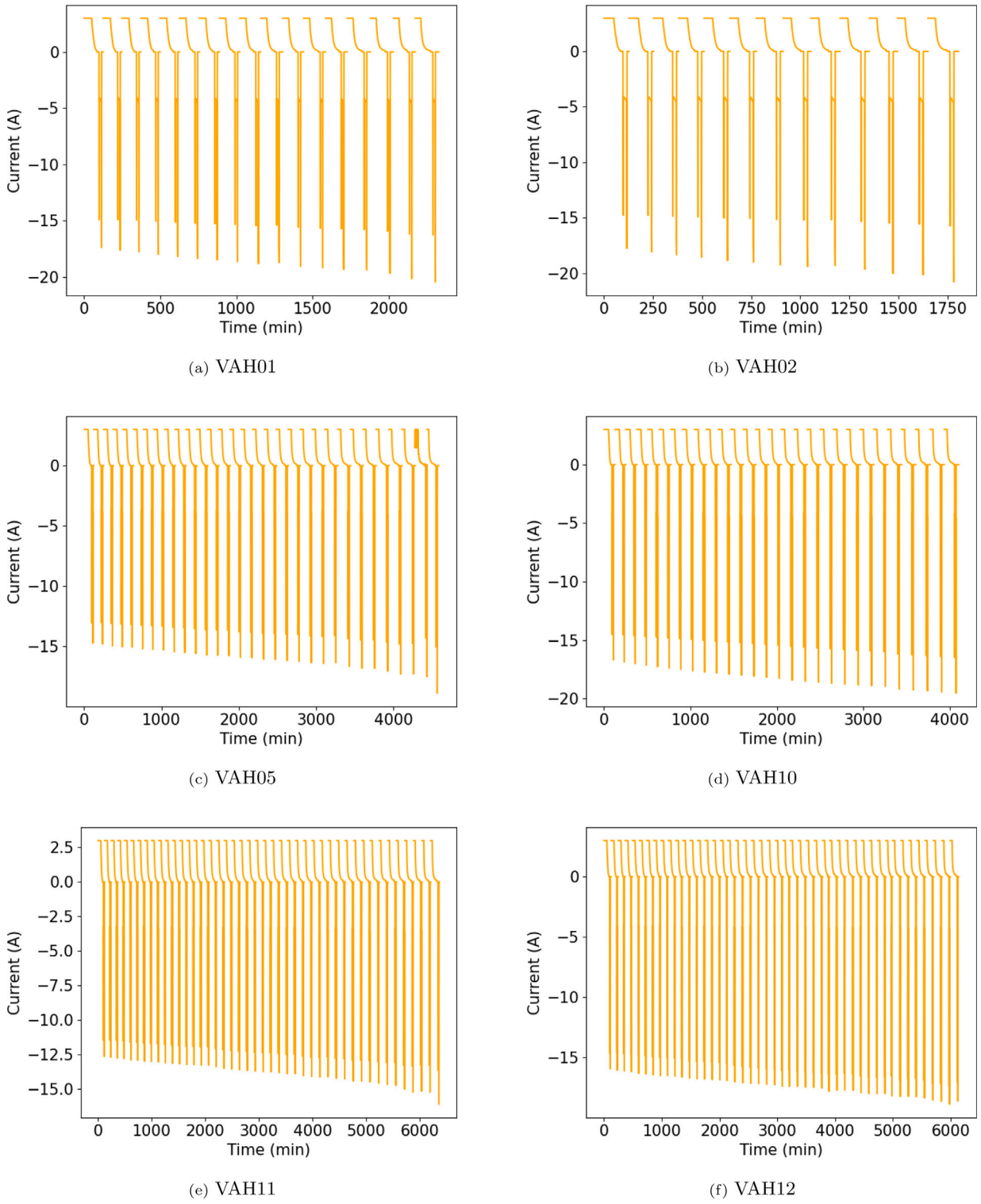

Fig. 15. Current during capacity tests for all 19 selected mission profiles.

the RUL estimation errors are below the average estimation errors. The change in the CC charging current is directly reflected in the change in the duration of the CC charging phase, i.e., an increase in the CC charging current leads to a decrease of the duration of the CC charging phase and vice versa. The importance of the CC charging current for RUL estimation is reflected by the fact that the CC charging phase duration, Δ^{CC}, is shown to have a high importance for RUL estimation (see Section 7.1). This is also in accordance with existing literature [50] where the CC charging duration is related to the battery's degradation. As the battery's capacity decreases gradually, it takes less time to fully charge the battery [51].

10. Conclusions

In this paper, a data-driven machine learning framework is proposed to predict the state of health and remaining useful lifetime of batteries

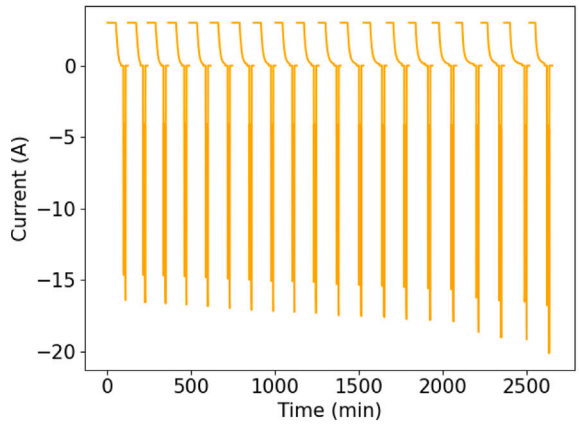

(g) VAH13

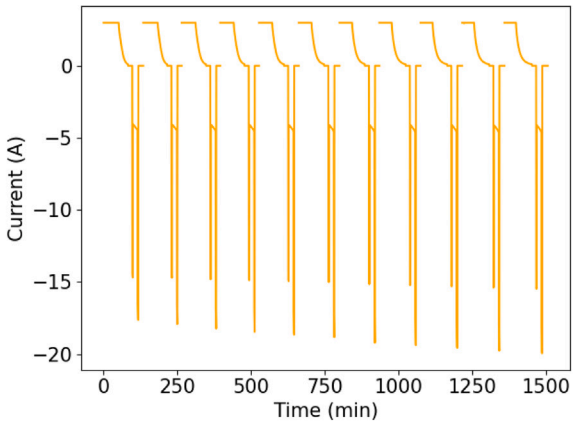

(h) VAH15

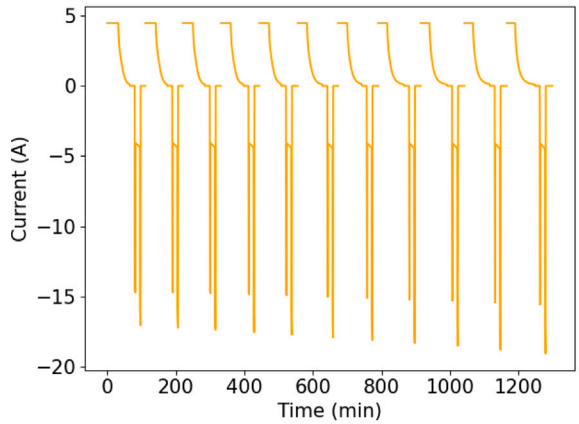

(i) VAH16

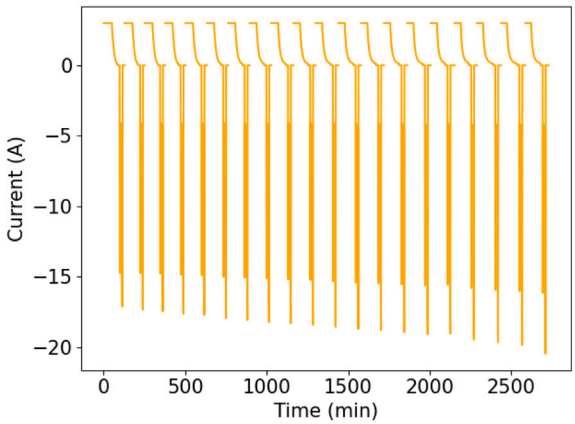

(j) VAH17

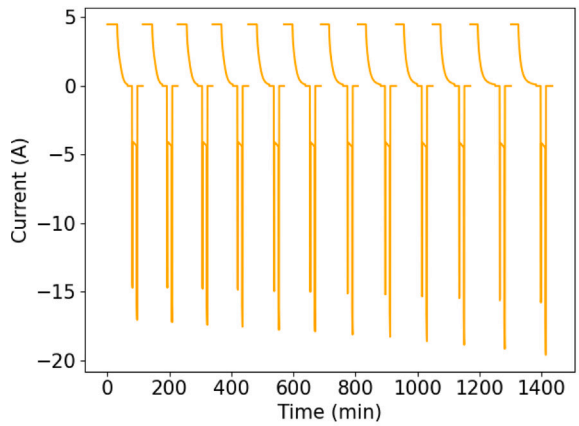

(k) VAH20

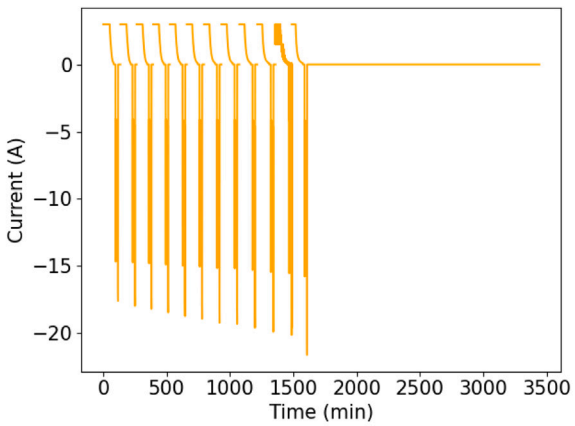

(l) VAH22

Fig. 15. (*continued*).

for Electric Vertical Take-off and Landing vehicles . We consider a dedicated dataset of batteries for Electric Vertical Take-off and Landing vehicles. These batteries are used to perform realistic flights. The flights are performed under varying conditions: temperature, cruise duration, discharge power, CC charging current and CV charging voltage. The Electric Vertical Take-off and Landing vehicles perform the take-off and landing at higher C-rates (5C-rate) than the cruise (1.48C-rate).

A total of 33 features have been generated based on charge-related, discharge-related, and temperature-related parameters. The importance of these features for state-of-health and remaining-useful-life estimation has been quantified. The results show that the features with the highest importance for state-of-health are the (variance, minimum) voltage recorded during take-off and the duration of the CC-CV charging phase. For RUL estimation, the voltage during take-off (variance, minimum), landing and cruise are of highest importance. The selected features for remaining-useful-life, but not for state-of-health estimation, are mean voltage during cruise and landing, maximum discharge capacity during cruise and landing, and variance discharge capacity during cruise.

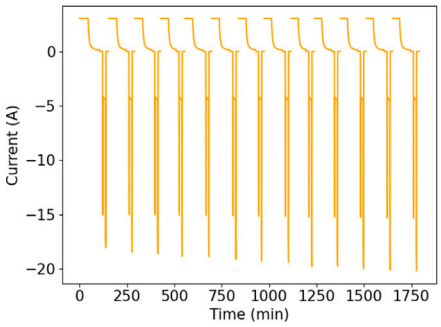

(m) VAH23

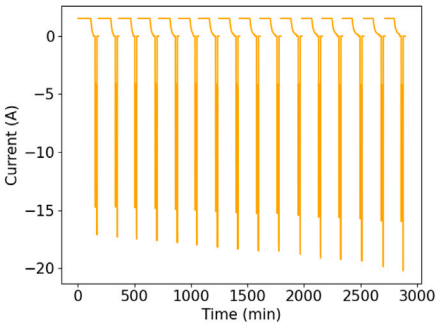

(n) VAH24

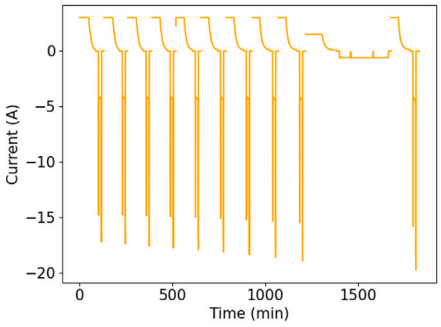

(o) VAH25

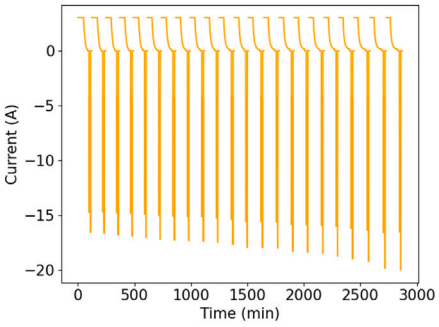

(p) VAH26

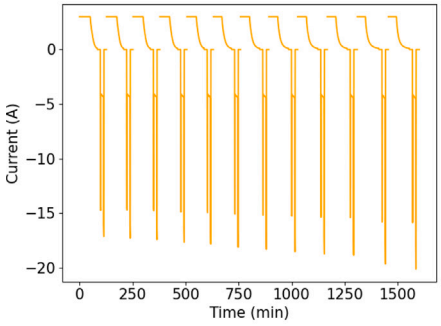

(q) VAH27

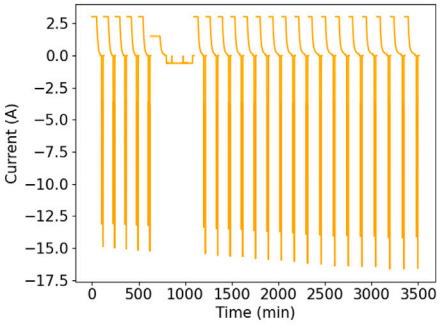

(r) VAH28

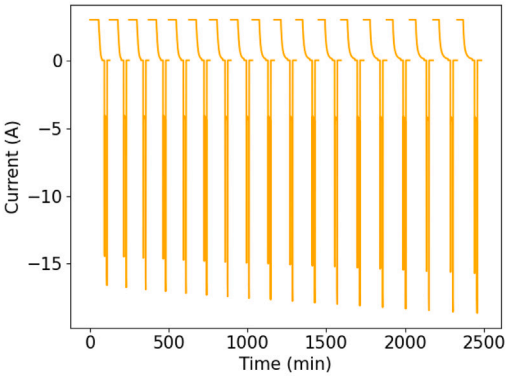

(s) VAH30

Fig. 15. (*continued*).

We have considered five machine learning algorithms for state-of-health and remaining-useful-life prognostics: Support Vector Machine, Random Forest regression, Extreme Gradient Boosting, Gaussian process regression, and Multilayer perceptron. The lowest state-of-health estimation errors are obtained using a Random forest regression (Mean Absolute Error= 1.33%). Extreme Gradient Boosting leads to the lowest remaining-useful-life estimation errors (Mean Absolute Error=54.33 missions). The results also show that when increasing the cruise duration by up to a 25%, the state-of-health and remaining-useful-life are well estimated by Random Forest regression and Extreme Gradient Boosting, respectively.

Declaration of competing interest

The authors declare that they have no known competing financial interests or personal relationships that could have appeared to influence the work reported in this paper.

Data availability

Data will be made available on request.

Appendix

See Fig. 15.

References

[1] Polaczyk N, Trombino E, Wei P, Mitici M. A review of current technology and research in urban on-demand air mobility applications. In: 8th biennial autonomous VTOL technical meeting and 6th annual electric VTOL symposium. 2019, p. 333–43.

[2] Fei Z, Yang F, Tsui K-L, Li L, Zhang Z. Early prediction of battery lifetime via a machine learning based framework. Energy 2021;225:120205.

[3] Shah FA, Sheikh SS, Mir UI, Athar SO. Battery health monitoring for commercialized electric vehicle batteries: Lithium-ion. In: 2019 international conference on power generation systems and renewable energy technologies. IEEE; 2019, p. 1–6.

[4] Tian H, Qin P, Li K, Zhao Z. A review of the state of health for lithium-ion batteries: Research status and suggestions. J Clean Prod 2020;261.

[5] Khalid M, Sheikh SS, Janjua AK, Khalid HA. Performance validation of electric vehicle's battery management system under state of charge estimation for lithium-ion battery. In: 2018 international conference on computing, electronic and electrical engineering. IEEE; 2018, p. 1–5.

[6] Mawonou KS, Eddahech A, Dumur D, Beauvois D, Godoy E. State-of-health estimators coupled to a random forest approach for lithium-ion battery aging factor ranking. J Power Sources 2021;484. http://dx.doi.org/10.1016/j.jpowsour.2020.229154.

[7] Zhang Y, Peng Z, Guan Y, Wu L. Prognostics of battery cycle life in the early-cycle stage based on hybrid model. Energy 2021;221:119901. http://dx.doi.org/10.1016/j.energy.2021.119901.

[8] Galiounas E, Tranter TG, Owen RE, Robinson JB, Shearing PR, Brett DJ. Battery state-of-charge estimation using machine learning analysis of ultrasonic signatures. Energy AI 2022;10:100188.

[9] Li J, Ziehm W, Kimball J, Landers R, Park J. Physical-based training data collection approach for data-driven lithium-ion battery state-of-charge prediction. Energy AI 2021;5:100094.

[10] Li Y, Liu K, M.Foley A, Zülke A, Berecibar M, Nanini-Maury E, et al. Data-driven health estimation and lifetime prediction of lithium-ion batteries: A review. Renew Sustain Energy Rev 2019;113.

[11] Xie R, Ma R, Pu S, Xu L, Zhao D, Huangfu Y. Prognostic for fuel cell based on particle filter and recurrent neural network fusion structure. Energy AI 2020;2:100017.

[12] Zraibi B, Okar C, Chaoui H, Mansouri M. Remaining useful life assessment for lithium-ion batteries using CNN-LSTM-DNN hybrid method. IEEE Trans Veh Technol 2021;70:4252–61.

[13] Du Z, Zuo L, Li J, Liu Y, Shen HT. Data-driven estimation of remaining useful lifetime and state of charge for lithium-ion battery. IEEE Trans Transp Electrification 2021;8:356–67.

[14] Mawonou KS, Eddahech A, Dumur D, Beauvois D, Godoy E. State-of-health estimators coupled to a random forest approach for lithium-ion battery aging factor ranking. J Power Sources 2021;484:229154.

[15] Liu Z, Zhao J, Wang H, Yang C. A new lithium-ion battery SOH estimation method based on an indirect enhanced health indicator and support vector regression in PHMs. Energies 2020;13:830.

[16] Li Y, Zou C, Berecibar M, Nanini-Maury E, Chan JC-W, Van den Bossche P, et al. Random forest regression for online capacity estimation of lithium-ion batteries. Appl Energy 2018;232:197–210.

[17] Tian J, Xiong R, Shen W. State-of-health estimation based on differential temperature for lithium ion batteries. IEEE Trans Power Electron 2020;35:10363–73.

[18] Attia P, Grover A, e. a. Jin N. Closed-loop optimization of fast-charging protocols for batteries with machine learning. Nature 2020;578:397–402.

[19] Bole B, Kulkarni C, Daigle M. Adaptation of an electrochemistry-based Li-ion battery model to account for deterioration observed under randomized use. In: Annual conference of the prognostics and health management society. 2014.

[20] Saha B, Goebel K. Battery data set, NASA Ames Prognostics Data Repository. 2017, (http://ti.arc.nasa.gov/project/prognostic-data-repository).

[21] Chen Z, Sun M, Shu X, Shen J, Xiao R. On-board state of health estimation for lithium-ion batteries based on random forest. In: IEEE international conference on industrial technology. 2018, p. 1754–9.

[22] Do. Reis G, Strange C, Yadav M, Li S. Lithium-ion battery data and where to find it. Energy AI 2021;5:100081.

[23] dos Reis G, Strange C, Yadav M, Li S. Lithium-ion battery data and where to find it. Energy AI 2021.

[24] Bills A, Viswanathan V, Sripad S, Frank E, Charles D, Fredericks WL. eVTOL battery dataset, ????. 2022, https://kilthub.cmu.edu/articles/dataset/eVTOL_Battery_Dataset/14226830?file=26855063. [Accessed 29 April 2022].

[25] Granado L, Ben-Marzouk M, Saenz ES, Boukal Y, Jugé S. Machine learning predictions of lithium-ion battery state-of-health for eVTOL applications. J Power Sources 2022;548:232051.

[26] Xiong R. Battery management algorithm for electric vehicles. Springer; 2020.

[27] Airbus. Vahana our single-set evtol demonstrator. 2019, https://www.airbus.com/en/urbanairmobility/vahana. [Accessed 10 May 2022].

[28] Bills A, Sripad S, Fredericks WL, Guttenberg M, Charles D, Frank E, et al. Universal battery performance and degradation model for electric aircraft. 2021.

[29] Roman D, Saxena S, Robu V, Pecht M, Flynn D. Machine learning pipeline for battery state-of-health estimation. Nat Mach Intell 2021;3:447–56.

[30] Severson KA, Attia PM, Jin N, Perkins N, Jiang B, Yang Z, et al. Data-driven prediction of battery cycle life before capacity degradation. Nature Energy 2019;4:383–91.

[31] Yang F, Wang D, Xu F, Huang Z, Tsui K-L. Lifespan prediction of lithium-ion batteries based on various extracted features and gradient boosting regression tree model. J Power Sources 2020;476.

[32] Zhang Y, Xiong R, He H, Pecht MG. Long short-term memory recurrent neural network for remaining useful life prediction of lithium-ion batteries. IEEE Trans Veh Technol 2018;67:5695–705.

[33] Sheikh SS, Anjum M, Khan MA, Hassan SA, Khalid HA, Gastli A, et al. A battery health monitoring method using machine learning: A data-driven approach. Energies 2020;13:3658.

[34] Alba-Maestre TS Javier, van Reine Koen Prud'homme, Castro SGP. Preliminary propulsion and power system design of a tandem-wing long-range eVTOL aircraft 11. 2021, p. 11083.

[35] Zhang C, Jiang J, Gao Y, Zhang W, Liu Q, Hu X. Charging optimization in lithium-ion batteries based on temperature rise and charge time. Appl Energy 2017;194:569–77.

[36] Pop V. Battery management systems : accurate state-of-charge indication for battery powered applications. Springer Ser. Philips research book series, V., vol. 9, 2008.

[37] Steinwart I, Christmann A. Support vector machines. Ser. information science and statistics, first ed.. Springer; 2008.

[38] Breiman L. Random forests. Mach Learn 2001;45:5–32.

[39] Li Y, Zou C, Berecibar M, Nanini-Maury E, Chan JC-W, van den Bossche P, et al. Random forest regression for online capacity estimation of lithium-ion batteries. Appl Energy 2018;232:197–210.

[40] Quinto B. Next-generation machine learning with spark. Springer; 2020.

[41] Richardson RR, Osborne MA, Howey DA. Gaussian process regression for forecasting battery state of health. J Power Sources 2017;357:209–19.

[42] Sharifzadeha M, Sikinioti-Lock A, Shah N. Machine-learning methods for integrated renewable power generation: A comparative study of artificial neural networks, support vector regression, and Gaussian process regression. Renew Sustain Energy Rev 2019;108:513–38.

[43] Yang D, Zhang X, Pan R, Wang Y, Chen Z. A novel Gaussian process regression model for state-of-health estimation of lithium-ion battery using charging curve. Appl Energy 2018;384:387–95.

[44] Hinton GE. Connectionist learning procedures. In: Machine learning III. 1990, p. 555–610.

[45] Lambelho M, Mitici M, Pickup S, Marsden A. Assessing strategic flight schedules at an airport using machine learning-based flight delay and cancellation predictions. J Air Transp Manag 2020;82:101737.

[46] Huang S-C, Tseng K-H, Liang J-W, Chang C-L, Pecht MG. An online SOC and SoH estimation model for lithium-ion batteries. Energies 2017;10:512.

[47] Bergstra J, Yamins D, Cox DD. Making a science of model search: Hyperparameter optimization in hundreds of dimensions for vision architectures. In: Proceedings of the 30th international conference on international conference on machine learning. Volume 28, ICML'13, JMLR.Org; 2013.

[48] Leng F, Tan CM, Pecht M. Effect of temperature on the aging rate of Li ion battery operating above room temperature. Sci Rep 2015;5.

[49] Lv S, Wang X, Lu W, Zhang J, Ni H. The influence of temperature on the capacity of lithium ion batteries with different anodes. Energies 2022;15:60.

[50] Keil P, Jossen A. Charging protocols for lithium-ion batteries and their impact on cycle life–An experimental study with different 18650 high-power cells. J Energy Storage 2016;6:125–41.

[51] Yang A, Wang Y, Yang F, Wang D, Zi Y, Tsui KL, et al. A comprehensive investigation of lithium-ion battery degradation performance at different discharge rates. J Power Sources 2019;443.